Monthly Notices
of the
ROYAL ASTRONOMICAL SOCIETY

Mon. Not. R. Astron. Soc. **417,** 2104–2123 (2011) doi:10.1111/j.1365-2966.2011.19393.x

The great escape: how exoplanets and smaller bodies desert dying stars

Dimitri Veras,★ Mark C. Wyatt, Alexander J. Mustill, Amy Bonsor and John J. Eldridge

Institute of Astronomy, University of Cambridge, Madingley Road, Cambridge CB3 0HA

Accepted 2011 July 6. Received 2011 June 26; in original form 2011 May 29

ABSTRACT

Mounting discoveries of extrasolar planets orbiting post-main-sequence stars motivate studies to understand the fate of these planets. In the traditional 'adiabatic' approximation, a secondary's eccentricity remains constant during stellar mass-loss. Here, we remove this approximation, investigate the full two-body point-mass problem with isotropic mass-loss, and illustrate the resulting dynamical evolution. The magnitude and duration of a star's mass-loss combined with a secondary's initial orbital characteristics might provoke ejection, modest eccentricity pumping, or even circularization of the orbit. We conclude that Oort Clouds and wide-separation planets may be dynamically ejected from 1–7 $M_\odot$ parent stars during AGB evolution. The vast majority of planetary material that survives a supernova from a 7–20 $M_\odot$ progenitor will be dynamically ejected from the system, placing limits on the existence of first-generation pulsar planets. Planets around $>20\,M_\odot$ black hole progenitors may easily survive or readily be ejected depending on the core collapse and superwind models applied. Material ejected during stellar evolution might contribute significantly to the free-floating planetary population.

Key words: Oort Cloud – planets and satellites: dynamical evolution and stability – planet–star interactions – stars: AGB and post-AGB – stars: evolution – supernovae: general.

1 INTRODUCTION

Understanding the formation and subsequent dynamical evolution of exoplanets has been a motivational hallmark for many observational and theoretical investigations. However, extrasolar planets continue to be discovered in surprising and exotic environments, and questions about the *endstate* of exoplanets are becoming increasingly relevant. Few studies so far have modelled these systems, which often feature evolved and variable parent stars. The rich dynamics therein fundamentally differ from studies of planets around main-sequence stars.

Examples of exoplanets which do not orbit main-sequence stars are growing. The first confirmed extrasolar planets were discovered around a neutron star: specifically, the millisecond pulsar PSR1257+12 (Wolszczan & Frail 1992; Wolszczan 1994). The minimum masses of these three planets continue to be among the lowest known to date, and two of these planets resonantly interact. Sigurdsson et al. (2003) later discovered another pulsar planet, around the binary radio millisecond pulsar PSR B1620−26. Exoplanets are also thought to orbit white dwarfs and stars with white dwarf companions. In the first category, GD 66 (Mullally et al. 2008, 2009), GD 356 (Wickramasinghe et al. 2010) and Gliese 3483 (Matt Burleigh, private communication) are planet-hosting stars. In the second category, examples are thought to include Gl 86 = HD 13445 (Queloz et al. 2000; Mugrauer & Neuhäuser 2005; Lagrange et al. 2006), HD 27442 (Butler et al. 2001; Chauvin et al. 2006), and HD 147513 (Mayor et al. 2004; Desidera & Barbieri 2007).

Additionally, planets have been discovered orbiting stars that have moved away from the main sequence but are not yet stellar remnants. Silvotti et al. (2007) discovered a giant planet orbiting the extreme horizontal branch star V 391 Pegasi, Geier et al. (2009) found a planet around the hot subdwarf star HD 149382, Lee et al. (2009) reported circumbinary planets to the sdB+M eclipsing system HW Virginis, and Setiawan et al. (2010) suggested that the planet orbiting the red horizontal branch star HIP 13044b might be of extragalactic origin. Cataclysmic variables are another class of systems which might harbour planets, and recently, planets around the cataclysmic variables QS Vir (Qian et al. 2010a), DP Leo (Qian et al. 2010b), HU Aqr (Qian et al. 2011) and DP Leonis (Beuermann et al. 2011) have been reported.

Prospects for discovering additional planets orbiting white dwarfs (Drake et al. 2010; Faedi et al. 2011) and extreme horizontal branch stars (Bear & Soker 2011) are promising, and observational campaigns to do so have already been initiated (Hogan, Burleigh & Clarke 2009; Benatti et al. 2010; Schuh et al. 2010). The *Kepler* mission can detect even smaller bodies around white dwarfs (Di Stefano, Howell & Kawaler 2010).

★E-mail: veras@ast.cam.ac.uk

Theoretical investigations of the evolution of planets around post-main-sequence stars have focused primarily on planet engulfment and interaction with the expanding stellar envelope, both for exoplanets and, specifically, for the Earth. Villaver & Livio (2007, 2009), Massarotti (2008) and Nordhaus et al. (2010) use particular stellar evolutionary tracks to determine ranges of semimajor axes at which planets are likely to be engulfed. In this regime, tidal modelling has a significant effect on the subsequent orbital evolution. However, as summarized by Hansen (2010), the nature of tidal dissipation is poorly understood and continues to yield different results depending on the model and assumptions used. For this reason, the fate of the Earth is uncertain. Sackmann, Boothroyd & Kraemer (1993), Rybicki & Denis (2001), Schröder & Connon Smith (2008) and Iorio (2010) – all explore the fate of the Earth in light of the Sun's post-main-sequence mass-loss, with differing results. Alternatively, Debes & Sigurdsson (2002) focus on the stability of multiplanet systems and link stellar mass-loss to instability time-scales. By doing so, they demonstrate how multiple planets beyond the reach of the star's expanding envelope might become unstable.

In this study, we consider just a single planet, or a smaller body. We perform a detailed analysis of the variable-mass two-body problem and apply the results to a wide range of star–planet fates that encompass all stellar masses $\lesssim 150\,\mathrm{M}_{\odot}$. We focus on how stellar mass-loss affects the eccentricity of a planet or planetary material, a link often ignored in previous studies. As a result, we show that planetary material can be ejected from a system based on mass-loss alone. We then quantify for what combination of parameters can we expect this behaviour.

We start, in Section 2, by reviewing the history of the variable-mass two-body problem and the corresponding equations of motion. We then analyse the orbital evolution in different mass-loss regimes, determine where and when the traditionally used adiabatic approximation holds, and estimate when the planets would become unstable. In Section 3, we apply the theory to stars of all masses up to $150\,\mathrm{M}_{\odot}$ in order to pinpoint realistic systems which would yield instability. We treat five different mass regimes in separate subsections. We then discuss the caveats, implications and potential extensions in Section 4, and conclude in Section 5.

2 THE GENERAL TWO-BODY MASS-LOSS PROBLEM

2.1 Overview

Mass-loss in the two-body problem, where both bodies are considered to be point masses, has been studied for over a century (e.g. Gyldén 1884; Mestschersky 1893). This situation is sometimes referred to as the 'Gyldén–Mestschersky' problem, even though this particular case refers to the situation that both the variable mass rates have the same functional dependence. The more general problem takes many forms, or special cases, which are nicely outlined by table 1 of Razbitnaya (1985). One well-known form results from the application of this general theory to binary stellar systems, a formalism pioneered by Jeans (1924). The mass-loss prescription that is named after him, $\dot{M} = -\kappa M^{j}$, where M is mass and κ and j are constants, has been analytically and numerically treated in many subsequent studies. However, specific applications of mass-loss to planetary systems have received little attention.

Soon after the advent of computer-based numerical integrations, Hadjidemetriou (1963, 1966a,b) revisited and reformulated the problem in important ways. Hadjidemetriou (1963) highlighted the subtlety with which mass-loss must be treated in order to retain physical interpretations of the evolution of orbital elements. He modelled mass-loss as an additional acceleration that is a function of a time- and mass-dependent velocity, and showed that for any isotropic mass-loss prescription, a planet's angular momentum h satisfies

$$h = \text{constant} = \sqrt{G\mu a\left(1-e^{2}\right)}, \tag{1}$$

where a refers to the semimajor axis, e to the eccentricity, and $\mu \equiv M_{\star} + M$. The subscript '$\star$' refers to the star and the variables without subscripts refer to the (lower-mass) secondary in the two-body system, which can be thought of as either a planet or a particle; we will use the term 'planet'. Despite the conservation of angular momentum, no such claim of conservation could be made about the total energy of the system.[1] Hadjidemetriou (1966b) then significantly discovered that amidst great mass-loss, such as in a supernova, the eccentricity of the secondary may increase, and eventually lead to ejection from the system. That finding is the foundation for this work. A subsequent series of papers (Verhulst 1969; Verhulst & Eckhaus 1970; Verhulst 1972) provided an expansion of and comparison with Hadjidemetriou's results. Alcock, Fristrom & Siegelman (1986) then approached the ejection possibilities from a different perspective by considering the effect of vigorous mass-loss of white dwarf progenitors on a comet. Later, Parriott & Alcock (1998) demonstrated how the asymmetric mass-loss case yields a greater fraction of cometary ejections.

Despite the large body of work on mass-loss in the two-body problem,[2] most studies continued to concentrate on binary stars. Debes & Sigurdsson (2002) helped break this trend by analysing the planetary case through the modelling of multiple planets orbiting a single star. They assumed that the planets had equal masses and initially circular orbits, and studied their motion in the 'adiabatic' approximation. This approximation holds when the *mass-loss time-scale is much greater than a planetary orbital time-scale*. In this approximation, the planet's eccentricity is thought to remain nearly constant, and hence, from equation (1),

$$\left(\frac{\mathrm{d}a}{\mathrm{d}t}\right)_{\text{adiabatic}} = -\frac{a}{\mu}\frac{\mathrm{d}\mu}{\mathrm{d}t}. \tag{2}$$

However, in the general planetary case, the angular momentum is a function of eccentricity, which is generally not constrained to be fixed. Other complicating factors are as follows.

(i) Because planetary orbits which are changing due to stellar mass-loss are not closed, averaged orbital element expressions can be misleading and counterintuitive, even though technically correct (Iorio 2010).

(ii) In a single phase of stellar evolution, mass-loss is typically non-constant (although monotonic) and may not be isotropic.

(iii) Stellar mass evolution typically involves multiple phases of mass-loss on time-scales which can vary by orders of magnitude.

(iv) Several additional forces due to stellar evolution, such as tides and dynamical friction from the expanding envelope, might be necessary to model in order to describe the correct orbital evolution.

[1] Because a system with isotropic mass-loss will maintain its rotational symmetry, according to Noether's Theorem, the angular momentum will be conserved. Because the same system does not exhibit time invariance, the energy of the system is not guaranteed to be conserved.

[2] Rahoma, Abd El-Salam & Ahmed (2009) provides a detailed summary of additional results from past papers, and Plastino & Muzzio (1992) summarizes the 'use and abuse' of using a force to model mass-loss.

Here, we do not place restrictions a planet's semimajor axis, eccentricity or orbital angles, but we do take measures to focus on our results. We treat mass-loss as isotropic. Tidal effects are unimportant in the regimes we consider here, and so we can safely ignore those. To foster intuition for the mass-loss problem, and to obtain tractable results, our analytics assume a constant mass-loss rate throughout. However, some of our analytical results are completely independent of the mass-loss rate assumed. The parameters for the example cases used in this section were selected to best demonstrate different aspects of the motion of this general two-body problem with mass-loss; more realistic cases are presented in Section 3. There, we apply the theory presented here to just a single phase of stellar evolution, but do consider almost the entire phase space of stellar mass.

2.2 Statement of equations

Although the equations of motion in terms of orbital elements for the variable-mass two-body problem can be derived from first principles, only a few authors (e.g. Hadjidemetriou 1963; Verhulst 1969; Deprit 1983; Li 2008) have stated them in full without averaging or approximation:

$$\frac{\mathrm{d}a}{\mathrm{d}t} = -\frac{a\left(1+e^2+2e\cos f\right)}{1-e^2}\frac{1}{\mu}\frac{\mathrm{d}\mu}{\mathrm{d}t}, \tag{3}$$

$$\frac{\mathrm{d}e}{\mathrm{d}t} = -\left(e+\cos f\right)\frac{1}{\mu}\frac{\mathrm{d}\mu}{\mathrm{d}t}, \tag{4}$$

$$\frac{\mathrm{d}i}{\mathrm{d}t} = \frac{\mathrm{d}\Omega}{\mathrm{d}t} = 0, \tag{5}$$

$$\frac{\mathrm{d}\omega}{\mathrm{d}t} = \frac{\mathrm{d}\varpi}{\mathrm{d}t} = -\frac{\sin f}{e}\frac{1}{\mu}\frac{\mathrm{d}\mu}{\mathrm{d}t}, \tag{6}$$

$$\frac{\mathrm{d}f}{\mathrm{d}t} = -\frac{\mathrm{d}\varpi}{\mathrm{d}t} + \frac{n\left(1+e\cos f\right)^2}{\left(1-e^2\right)^{3/2}}. \tag{7}$$

where i is inclination, Ω is the longitude of ascending node, ϖ is the longitude of pericentre, ω is the argument of pericentre and f is the true anomaly. Equations (1), (3) and (4) are self-consistent and may be derived from one another with the help of the *vis viva* equation. The time derivative of position in terms of orbital elements and the statement of the conservation of angular momentum in polar coordinates give equations (6) and (7), respectively.

These equations may also be derived from more general considerations. Gauge theory is a basis from which one may obtain sets of equations such as Lagrange's planetary equations and Gauss' planetary equations by defining just a single perturbative acceleration to the classic two-body problem, and a gauge velocity. The formulation of the theory with regard to planetary dynamics as well as extensive descriptions can be found in Efroimsky & Goldreich (2003, 2004), Gurfil (2004), Efroimsky (2005a), Efroimsky (2005b, 2006), Gurfil (2007) and Gurfil & Belyanin (2008). Hadjidemetriou (1963) showed that the sum of the isotropic mass variation of both bodies is equivalent to a perturbative force with an acceleration of $\Delta \boldsymbol{A} = -(1/2)(\mathrm{d}\mu/\mathrm{d}t)(1/\mu)\boldsymbol{v}$, where $\boldsymbol{v}$ is velocity. This acceleration yields equations (3)–(7) directly for a zero gauge.

Every variable in equations (3)–(7) is considered to be a function of time. The mean motion, n, is equal to $G^{1/2}\mu^{1/2}/a^{3/2}$, where G is treated as the standard gravitational constant. Although we use μ throughout this work to emphasize how the motion is affected by the sum of the mass-loss (or gained) by both bodies, the value of the planetary mass and how it changes with time have a negligible effect on the results for $M_\star \gg M$. For a 1 $\mathrm{M}_\odot$ star, if one assumes a planetary mass of $\sim$10 Jupiter masses, which is of the order of the theoretical upper bound, then $M/M_\star \sim 1$ per cent.

The planet's true longitude, θ, varies according to

$$\frac{\mathrm{d}\theta}{\mathrm{d}t} = \frac{n\left(1+e\cos f\right)^2}{\left(1-e^2\right)^{3/2}}, \tag{8}$$

which is not explicitly dependent on the mass-loss rate and hence is equivalent to the case of no mass-loss. This equation demonstrates that from the point of view of a fixed reference direction, the secondary will continue to circulate around a star that is losing mass as long as the secondary remains bound.

For completeness, we consider the evolution of other traditionally used orbital parameters. The planet's eccentric anomaly, E, will vary according to

$$\frac{\mathrm{d}E}{\mathrm{d}t} = \frac{n\left(1+e\cos f\right)}{1-e^2} + \frac{\sin f}{e\sqrt{1-e^2}}\frac{1}{\mu}\frac{\mathrm{d}\mu}{\mathrm{d}t}. \tag{9}$$

Note that the right-hand sides of equations (3)–(9) may be expressed in terms of the eccentric anomaly instead of the true anomaly. The planet's mean motion will vary according to

$$\frac{\mathrm{d}n}{\mathrm{d}t} = \frac{n\left(2+e^2+3e\cos f\right)}{1-e^2}\frac{1}{\mu}\frac{\mathrm{d}\mu}{\mathrm{d}t}. \tag{10}$$

The planet's mean anomaly, Π, can be expressed as an explicit function of time by use of the 'time of pericentre', τ:

$$\frac{\mathrm{d}\Pi}{\mathrm{d}t} = n + n\left(t-\tau\right)\frac{\left(2+e^2+3e\cos f\right)}{1-e^2}\frac{1}{\mu}\frac{\mathrm{d}\mu}{\mathrm{d}t} \tag{11}$$

or, through Kepler's equation, as

$$\frac{\mathrm{d}\Pi}{\mathrm{d}t} = n + \frac{\sqrt{1-e^2}\sin f\left(1+e^2+e\cos f\right)}{e\left(1+e\cos f\right)}\frac{1}{\mu}\frac{\mathrm{d}\mu}{\mathrm{d}t}, \tag{12}$$

which is explicitly independent of time. Finally, the mean longitude, λ, changes with time according to

$$\frac{\mathrm{d}\lambda}{\mathrm{d}t} = \frac{\mathrm{d}\Pi}{\mathrm{d}t} + \frac{\mathrm{d}\varpi}{\mathrm{d}t} = n - \frac{\mathrm{d}\varpi}{\mathrm{d}t}\left[\frac{\sqrt{1-e^2}\left(1+e^2+e\cos f\right)}{1+e\cos f} - 1\right]. \tag{13}$$

Throughout this paper, we denote initial values by the subscript '0'.

2.3 Parametrizing mass-loss

Suppose the mass-loss rate is constant and equal to $-\alpha$, such that $\alpha > 0$. Then $\mu = G(\mu_0 - \alpha t)$, and

$$\frac{1}{\mu}\frac{\mathrm{d}\mu}{\mathrm{d}t} = -\left(\frac{\mu_0}{\alpha} - t\right)^{-1}. \tag{14}$$

We can better quantify adiabaticity and various regimes of motion due to mass-loss by defining a dimensionless 'mass-loss index', Ψ:

$$\Psi \equiv \frac{\alpha}{n\mu} = \frac{1}{2\pi}\left(\frac{\alpha}{1\,\mathrm{M}_\odot\,\mathrm{yr}^{-1}}\right)\left(\frac{a}{1\,\mathrm{au}}\right)^{3/2}\left(\frac{\mu}{1\,\mathrm{M}_\odot}\right)^{-(3/2)}. \tag{15}$$

This parameter provides a scaled ratio of the orbital period to the mass-loss time-scale. The initial value of the index is Ψ_0. Hence, the time evolution of Ψ is governed by

$$\frac{\mathrm{d}\Psi}{\mathrm{d}t} = -3\Psi\left(\frac{1+e\cos f}{1-e^2}\right)\frac{1}{\mu}\frac{\mathrm{d}\mu}{\mathrm{d}t}. \tag{16}$$

When $\Psi \ll 1$, a system can be considered 'adiabatic' – the case we treat first.

2.4 'Adiabatic' regime evolution

2.4.1 Adiabatic eccentricity evolution

We begin with analysing the equations of motion by first considering equation (4), because all non-zero equations of motion explicitly include e in some manner. Note importantly that the equation demonstrates that an initially circular planet will not remain on a circular orbit, and that the planet's eccentricity will undergo oscillations on orbital time-scales when the parent star loses mass.

We can solve equation (4) by noting that in the adiabatic approximation ($\Psi \ll 1$), the first term in equation (7) is considered to be negligible compared to the second term ($= \mathrm{d}\theta/\mathrm{d}t$), because the first term is proportional to the mass-loss rate. Further, μ is assumed to remain fixed over the course of one orbit. Hence, in this regime, equation (4) may be integrated directly over the true anomaly, with the result

$$e_{\mathrm{adiabatic}} = e_0 + \Psi_0 \frac{\left(1 - e_0^2\right)^{3/2} \sin f}{1 - e_0 \cos f}. \tag{17}$$

According to equation (17), after each orbit the eccentricity will return to its initial value. During the orbit, the amplitude of $(e_{\mathrm{adiabatic}} - e_0)$ is $\Psi_0(1 - e_0^2) \propto \alpha$. Thus, assuming a current value of $\alpha_\odot \approx 10^{-13}\,\mathrm{yr}^{-1}$, the Earth's eccentricity is raised by about 10^{-14} each year due to the Sun's mass-loss.

Fig. 1 demonstrates the accuracy of equation (17) when compared with the evolution from the full equations of motion (equations 3–7) for a $a_{\mathrm{o}} = 1$ au planet orbiting a $\mu_0 = 1\,\mathrm{M}_\odot$ star which is losing mass at the rate of $10^{-5}\,\mathrm{M}_\odot\,\mathrm{yr}^{-1}$ (8 orders of magnitude greater than $\alpha_\odot$). The agreement is excellent over the course of a single orbit. Over time, the approximation gradually worsens, as the evolution of Ψ_0 is not taken into account in equation (17).

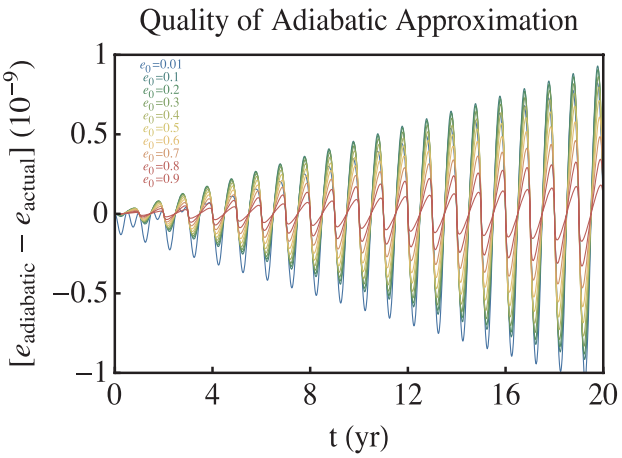

Figure 1. Analytic approximation to the eccentricity evolution in the adiabatic regime. Shown here is the difference in eccentricity of a planet evolving according to equation (17) compared to equations (3)–(7). The planet is located at $a_0 = 1$ au from a $\mu_0 = 1\,\mathrm{M}_\odot$ star that is losing mass at the rate of a rate of $\alpha = 10^{-5}\,\mathrm{M}_\odot\,\mathrm{yr}^{-1}$ ($\Psi_0 \approx 1.6 \times 10^{-6}$). The differently coloured lines from the top of each crest moving downwards correspond to $e_0 = 0.01$, 0.1, 0.2, 0.3, 0.4, 0.5, 0.6, 0.7, 0.8 and 0.9, respectively.

2.4.2 Adiabatic semimajor axis evolution

We now consider the semimajor axis evolution from equation (3). Note from the equation that for any mass-loss, the semimajor axis can never decrease.

In the adiabatic regime, the semimajor axis is traditionally evolved according to equation (2). Note, however, that the equation does not follow from equation (3) if $e \neq 0$. Yet, when the semimajor axis is averaged over one orbital period, the eccentricity terms vanish and equation (2) is recovered. The solution of this equation is

$$a_{\mathrm{adiabatic}} = a_0 \left(1 - \frac{\alpha t}{\mu_0}\right)^{-1}. \tag{18}$$

Therefore, an adiabatically evolving planet will, for example, double its orbital separation if its parent $1\,\mathrm{M}_\odot$ star constantly loses mass at the rate of $\alpha = 5 \times 10^{-9}\,\mathrm{M}_\odot\,\mathrm{yr}^{-1}$ over 100 Myr. In a different example, a $2\,\mathrm{M}_\odot$ star is expected to lose at most ≈70 per cent of its initial mass. Therefore, *if* all this mass is lost adiabatically, then orbiting planets can expect to increase their semimajor axis by at most a factor of ≈3.3.

2.4.3 Adiabatic orbital angle evolution

Turning to other orbital parameters, the longitude of pericentre is a typically secular feature of multiplanet extrasolar systems. Its variational time-scale is often of the order of thousands of orbits. During stellar evolution, however, equation (6) demonstrates that the variation in a planet's longitude of pericentre is quick (on orbital time-scales), and changes sign over each orbital period. To be consistent with the adiabatic approximation, in which $\mathrm{d}\omega/\mathrm{d}t \approx 0$ in equation (7), then

$$\varpi_{\mathrm{adiabatic}} = \varpi_0. \tag{19}$$

Because $\mathrm{d}\varpi/\mathrm{d}t$ is assumed to be zero, the value of $f_{\mathrm{adiabatic}}$ follows the same evolution as f would in the two-body problem with no mass-loss.

We can obtain an adiabat for n from equation (10) under the same assumptions that were used to derive equations (2) and (18):

$$n_{\mathrm{adiabatic}} = n_0 \left(1 - \frac{\alpha t}{\mu_0}\right)^{2}. \tag{20}$$

Thus, in the adiabatic approximation, the mean motion is a monotonically decreasing function. In the same example system from Section 2.4.2, with $\mu_0 = 1\,\mathrm{M}_\odot$, and $\alpha = 5 \times 10^{-9}\,\mathrm{M}_\odot\,\mathrm{yr}^{-1}$, after $t = 100$ Myr the planet's mean motion would decrease by a factor of 4. This result is expected of Kepler's third law with a halved stellar mass and a doubled semimajor axis. For $2\,\mathrm{M}_\odot$ stars, the final Keplerian period of a planet when mass-loss has ceased would be enhanced from its initial period by a factor of at most ≈11.

2.4.4 Adiabatic evolution in space

In space, adiabatic evolution corresponds to a planet orbiting in an outward spiral pattern. Fig. 2 displays such an orbit (for $\Psi_0 \approx 0.0016$), which is not closed. After each cycle of true longitude, the eccentricity does return to its initial osculating value. The semimajor axis is seen to increase by as much as 10 per cent of a_0 per orbit. The increase in orbital period can be linked with the circulation time-scale of f.

A highly eccentric planet might make close passes to the star, close enough to be affected by tides and the stellar envelope. In

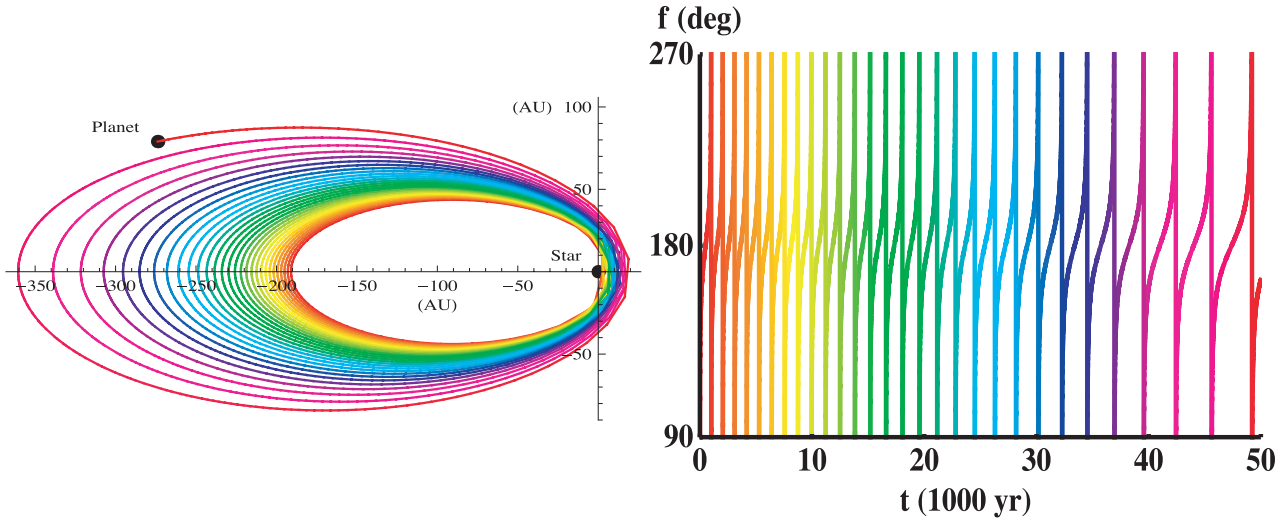

Figure 2. The adiabatic regime. The position in space (left-hand panel) and the evolution of the true anomaly (right-hand panel) of a planet (or belt particle) that is being pushed outward due to stellar mass-loss. The colours on the curves indicate evolution at the same points in time, and the vertical lines of true anomaly indicate circulations of the angle. The star has an initial mass of $\mu_0 = M_\star = 1\,\mathrm{M}_\odot$ and is losing mass at the rate of $\alpha = 1 \times 10^{-5}\,\mathrm{M}_\odot\,\mathrm{yr}^{-1}$. The planet begins on a highly eccentric orbit ($e_0 = 0.9$) at $a_0 = 100$ au, with $f_0 = 0^\circ$. Hence, $\Psi_0 = 0.0016$. Note that as the planet moves outwards and its mean motion decreases, the circulation period of the true anomaly decreases as well.

order to determine if the planet is more or less likely to suffer these encounters from mass-loss, consider the evolution of the pericentre, q, of the planet:

$$\frac{\mathrm{d}q}{\mathrm{d}t} = -\frac{a\,(1-e)\,(1-\cos f)}{1+e}\,\frac{1}{\mu}\,\frac{\mathrm{d}\mu}{\mathrm{d}t}. \tag{21}$$

Equation (21) demonstrates that the pericentre *monotonically increases with stellar mass-loss*. The left-hand panel of Fig. 2 corroborates this relation. Therefore, if a planet 'outruns' the star's expanding envelope, then one can ignore the envelope's influence on the planet.

2.5 Regime transition

2.5.1 The breaking of adiabaticity

Equation (20) has important implications for the dynamical system, as mean motion is inversely proportional to the Keplerian period. Hence, as a star loses mass, and pushes a planet radially outward, the mean motion decreases, and *eventually the orbital period will be comparable to the mass-loss time-scale* ($\Psi \sim 1$). More precisely, $\mathrm{d}\theta/\mathrm{d}t$ (which is proportional to the mean motion) will eventually become equal to $(-\mathrm{d}\varpi/\mathrm{d}t)$ (which is proportional to the mass-loss time-scale). At this bifurcation point in the dynamics, equation (7) demonstrates that the true anomaly becomes momentarily stationary. At this point, one can claim that adiabaticity is broken.

Note that in the adiabatic regime, f circulates. At and beyond the bifurcation point, $\mathrm{d}f/\mathrm{d}t$ instead begins to librate. The effect of a librating f on $\mathrm{d}a/\mathrm{d}t$ and $\mathrm{d}e/\mathrm{d}t$ is pronounced, quick and runaway. The eccentricity and semimajor axes evolution undergo a qualitative change, and the rate of increase in the latter is pronounced. Therefore, we denote this regime as the 'runaway' regime. We wish to investigate this regime transition, and do so first qualitatively through Figs 3 and 4. These figures model a $1\,\mathrm{M}_\odot$ star which is losing mass at a relatively high rate of $\alpha = 5 \times 10^{-5}\,\mathrm{M}_\odot\,\mathrm{yr}^{-1}$ over 1.5×10^4 yr. After this amount of time, the star will have lost 75 per cent of its initial mass. These values are chosen for demonstration purposes, as typical $1\,\mathrm{M}_\odot$ stars will lose ≈35–62 per cent of their mass en route to becoming a white dwarf. We model more realistic systems in Section 3.

Fig. 3 illustrates the approach to and onset of adiabaticity breaking, with $\Psi_0 = 0.023$ (left-hand panel) and $\Psi_0 = 0.25$ (right-hand panel). In the first case, the eccentricity ceases to remain approximately constant and can start to oscillate on the order of a 10th. In the second case, where Ψ quickly assumes values on the order of unity, planets evolve in the runaway regime and may achieve hyperbolic orbits.

Fig. 4 showcases the semimajor axis evolution for the same systems in Fig. 3. In the left-hand panel of Fig. 4, the curves of initial eccentricity break away from the adiabat, increasing at a steeper rate than the adiabat. In the right-hand panel, at $t = 0$, the systems are just beyond the adiabat and are 'running away' from the star. For a constant mass-loss that turns on and off nearly instantaneously (such as in a supernova), planets might not ever evolve adiabatically, and begin their life in the runaway regime. Note that unlike eccentricity, the semimajor axis is always increasing, even when oscillating about the adiabat. In the runaway regime, the departure from the adiabat is drastic; the right-hand panel shows that the planet may increase its semimajor axis by many factors before achieving a hyperbolic orbit.

The resulting increase in a will cause the mean motion term in equation (7) to decrease further. In the limiting case where $\mathrm{d}\omega/\mathrm{d}t \gg n$, the libration amplitude will approach zero, and the true anomaly will become nearly stationary. As a result, the $\cos f$ term in equation (4) becomes constant, and $\mathrm{d}e/\mathrm{d}t$ becomes linear in e, causing a positive feedback effect that is characteristic of the runaway regime.

An orbit that is transitioning out of adiabaticity will not complete its final orbit around the star, as the true anomaly is no longer circulating. Fig. 5 illustrates the resulting motion in space. The system selected is the highest eccentricity ($e_0 = 0.9$) curve from the left-hand panels of Figs 3 and 4 ($\Psi_0 = 0.023$). The system reaches the bifurcation point at $\approx 1.2 \times 10^4$ yr, as one can read from the right-hand panel. Now we explore this bifurcation point analytically.

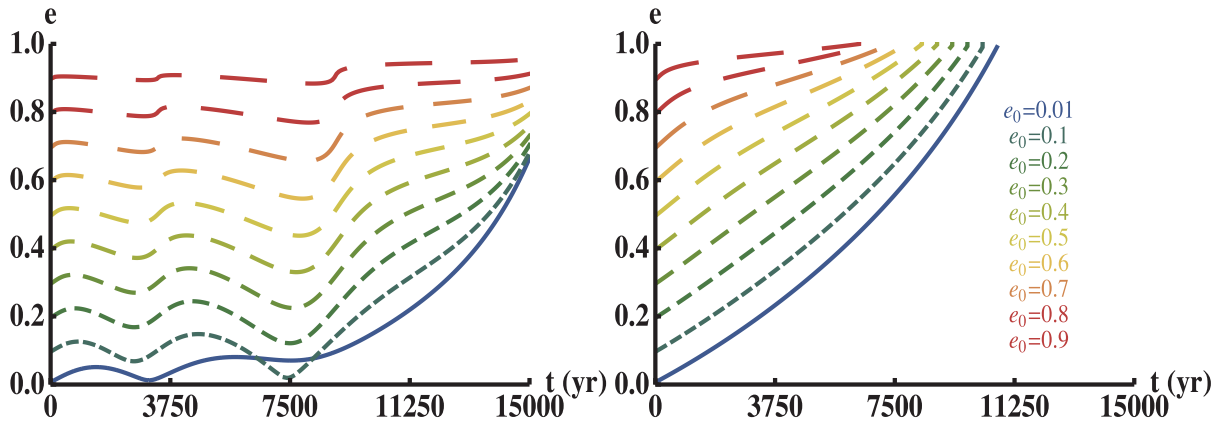

Figure 3. The breaking of adiabaticity. Shown is the eccentricity evolution over 10^4 yr of evolution of $a_0 = 200$ au planets (or belt particles; left-hand panel) and $a_0 = 10^3$ au planets (or belt particles; right-hand panel) orbiting a $\mu_0 = M_\star = 1\,\mathrm{M}_\odot$ star losing mass at a rate of $\alpha = 5 \times 10^{-5}\,\mathrm{M}_\odot\,\mathrm{yr}^{-1}$. The initial mass-loss index for the systems in the left- and right-hand panels are respectively $\Psi_0 \approx 0.023$ and 0.25, values that are close to the transition point in the dynamics between the adiabatic and runaway regimes. Here, $f_0 = 0^\circ$. The lines with an increasing dash length represent e_0 values of 0.01, 0.1, 0.2, 0.3, 0.4, 0.5, 0.6, 0.7, 0.8 and 0.9, respectively. In the right-hand panel, all planets are ejected from the system within 10^4 yr except the two planets with the lowest initial eccentricity.

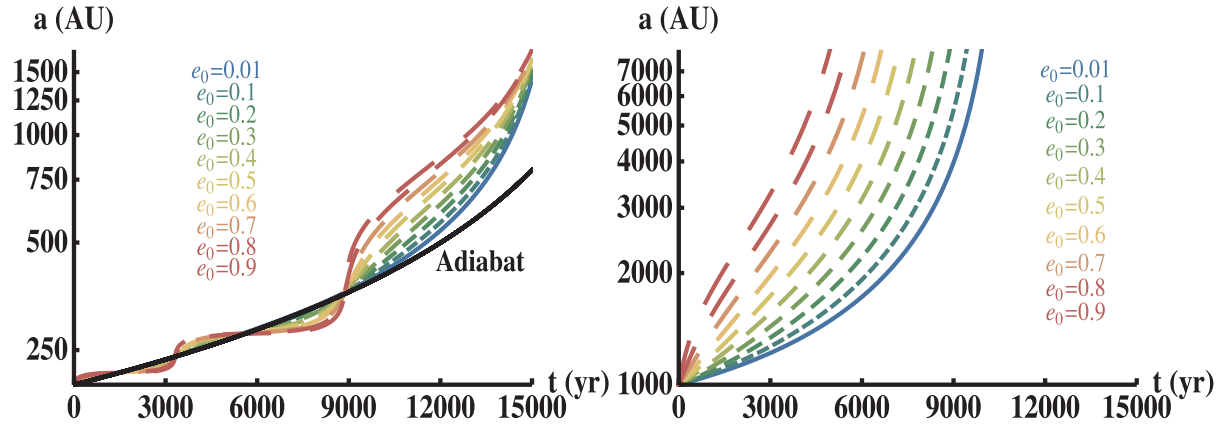

Figure 4. The breaking of adiabaticity for the same two systems in Fig. 3. In the left-hand panel, note how the eccentric planets oscillate about the adiabat until reaching the runaway regime. In the right-hand panel, the planets begin at $t = 0$ just off of the adiabat, and quickly settle into the runaway regime.

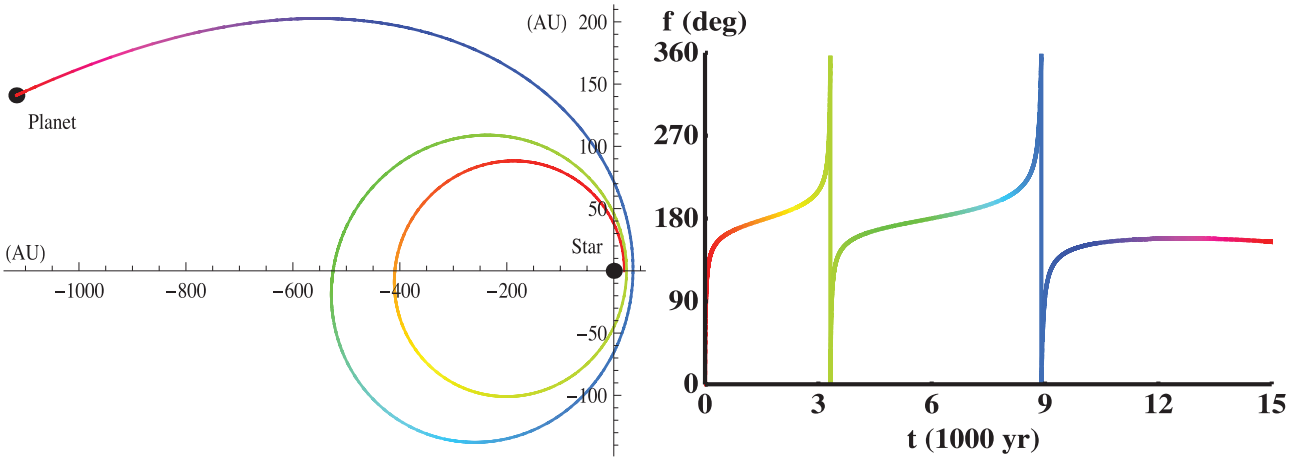

Figure 5. The position in space (left-hand panel) and the evolution of the true anomaly (right-hand panel) of the $e_0 = 0.9$ planet from the system in the left-hand panels of Figs 3 and 4. At $t \approx 1.2 \times 10^4$ yr, the planet stops circulating and starts to head out of the system as the true anomaly becomes stationary.

2.5.2 *Characterizing the bifurcation point*

The bifurcation point, as we defined in the last subsection, is the first moment when $\mathrm{d}\theta/\mathrm{d}t = -\mathrm{d}\varpi/\mathrm{d}t$. At this moment, from equation (7), $\mathrm{d}f/\mathrm{d}t = 0$, and

$$\Psi_{\rm bif} = \frac{e_{\rm bif}\,(1 + e_{\rm bif}\cos f_{\rm bif})^2}{\sin f_{\rm bif}\left(1 - e_{\rm bif}^2\right)^{3/2}}. \tag{22}$$

For the majority of possible values of eccentricity and true anomaly, $\Psi_{\rm bif} \approx 0.1$–$1.0$. There are an infinite number of triples $(\Psi_{\rm bif}, e_{\rm bif}, f_{\rm bif})$ that satisfy equation (22). We cannot determine any of these three values from the initial conditions, although one may approximate $e_{\rm bif} \approx e_0$ from the adiabatic approximation. However, at this point in the planet's evolution, $e_{\rm bif}$ might differ by over 0.1 from e_0.

The functional form of equation (22) suggests that for a given $\Psi_{\rm bif}$ and a given $e_{\rm bif}$, there might be more than one value of $f_{\rm bif}$ which satisfies the equation. We now investigate this possible multiplicity further by considering the extremities of $\Psi_{\rm bif}$ with respect to $e_{\rm bif}$ and $f_{\rm bif}$. There are six values of $f_{\rm bif}$ which satisfy $\mathrm{d}\Psi_{\rm bif}/\mathrm{d}f_{\rm bif} = 0$, five of which are unphysical. The one physical solution is

$$f_{\rm bif,min} = \cos^{-1}\left[\frac{1 - \sqrt{1 + 8e_{\rm bif}^2}}{2e_{\rm bif}}\right], \tag{23}$$

where $90^\circ \leq f_{\rm bif} \leq 270^\circ$. Let the value of $\Psi_{\rm bif}$ at $f_{\rm bif} = f_{\rm bif,min}$ be denoted by $\Psi_{\rm bif,fmin}$. Then, for a given $\Psi_{\rm bif}$ and a given $e_{\rm bif}$, the number of values of $f_{\rm bif}$ which satisfy equation (22) are

$$0 \quad \text{values of} \quad f_{\rm bif} \quad \text{if} \quad \Psi_{\rm bif} < \Psi_{\rm bif,fmin}, \tag{24}$$

$$1 \quad \text{value of} \quad f_{\rm bif} \quad \text{if} \quad \Psi_{\rm bif} = \Psi_{\rm bif,fmin}, \tag{25}$$

$$2 \quad \text{values of} \quad f_{\rm bif} \quad \text{if} \quad \Psi_{\rm bif} > \Psi_{\rm bif,fmin}. \tag{26}$$

The maximum value of $\Psi_{\rm bif,min}$ (obtained in the limit $e_{\rm bif} \to 1$) is $4/(3\sqrt{3})$. Therefore, for any given $\Psi_{\rm bif} > 4/(3\sqrt{3}) \approx 0.77$, there are two possible values of $f_{\rm bif}$ which satisfy equation (22). Fig. 6 demonstrates equations (24)–(26) graphically by plotting

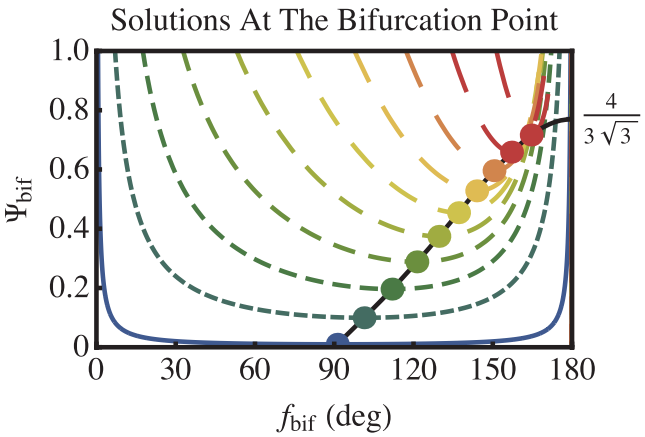

Figure 6. Values of $(\Psi_{\rm bif}, e_{\rm bif}, f_{\rm bif})$ at the bifurcation point, where lines with an increasing dash length represent $e_{\rm bif}$ values of 0.01, 0.1, 0.2, 0.3, 0.4, 0.5, 0.6, 0.7, 0.8 and 0.9, respectively. The corresponding colour dots represent the value of $\Psi_{\rm bif,fmin}$ for a given $e_{\rm bif}$, when just one value of $f_{\rm bif}$ satisfies equation (22). Adiabatic systems approaching the bifurcation point would be travelling upwards on this plot while circulating nearly parallel to the x-axis.

$\Psi_{\rm bif}$ versus $f_{\rm bif}$ for 10 values of $e_{\rm bif}$ (0.01, 0.1, 0.2, 0.3, 0.4, 0.5, 0.6, 0.7, 0.8 and 0.9). Large dots mark where $\Psi_{\rm bif} = \Psi_{\rm bif,fmin}$. As adiabatic systems increase Ψ and approach the bifurcation point, their evolution can be imagined as moving upwards in this plot while circulating almost parallelly to the x-axis. Eventually they will reach the bifurcation point, preferentially at $\Psi_{\rm bif,min}$.

Note from equation (22) that $e_{\rm bif} \to 0$ implies $\Psi_{\rm bif} \to 0$, suggesting that planets with initially circular orbits can never be in the adiabatic regime. However, this is not true. If $e_0 = 0$, then from equation (17), $e_{\rm adiabatic} = \Psi_0 \sin f$. Inserting this expression into equation (7) yields

$$\left.\frac{\mathrm{d}f}{\mathrm{d}t}\right|_{t=0,e_0=0} = n\left[\frac{\left(1 + \frac{1}{2}\Psi_0 \sin 2f\right)^2}{\left(1 - \Psi_0^2 \sin^2 f\right)^{3/2}} - 1\right] > 0 \tag{27}$$

for any non-zero value of f (f attains a positive value immediately even if $f_0 = 0$). After $t = 0$, $\mathrm{d}f/\mathrm{d}t$ will then continue to increase until the bifurcation point is reached. Therefore, initially circular planets may easily evolve adiabatically, which corroborates numerical simulations.

Now we consider $\mathrm{d}\Psi_{\rm bif}/\mathrm{d}e_{\rm bif} = 0$. There are three solutions, two of which are physical:

$$e_{\rm bif,ext1} = \frac{1}{4}\left(-3\cos f_{\rm bif} + \sqrt{-\frac{7}{2} + \frac{9}{2}\cos\left(2f_{\rm bif}\right)}\right), \tag{28}$$

$$e_{\rm bif,ext2} = \frac{1}{4}\left(-3\cos f_{\rm bif} - \sqrt{-\frac{7}{2} + \frac{9}{2}\cos\left(2f_{\rm bif}\right)}\right), \tag{29}$$

where $f_{\rm crit} \leq f_{\rm bif} \leq (360^\circ - f_{\rm crit})$, such that

$$f_{\rm crit} = 180^\circ - \frac{1}{2}\cos^{-1}\left(\frac{7}{9}\right) \approx 160.^\circ53. \tag{30}$$

This critical true anomaly value will be important for describing motion in the runaway regime because it determines where a qualitative change in the evolution occurs. For a given $\Psi_{\rm bif}$ and a given $f_{\rm bif}$, the numbers of values of $e_{\rm bif}$ that satisfy equation (22) are

$$1 \quad \text{value of} \quad e_{\rm bif} \quad \text{if} \quad 0^\circ \leq f_{\rm bif} < f_{\rm crit}, \tag{31}$$

$$3 \quad \text{values of} \quad e_{\rm bif} \quad \text{if} \quad f_{\rm crit} < f_{\rm bif} < 180^\circ, \tag{32}$$

$$\infty \quad \text{values of} \quad e_{\rm bif} \quad \text{if} \quad f_{\rm bif} = f_{\rm crit}. \tag{33}$$

The limiting values of $\Psi_{\rm bif}$ at $e_{\rm bif} = e_{\rm bif,ext1}$ and $e_{\rm bif} = e_{\rm bif,ext2}$ are $2/3$ and $4/(3\sqrt{3})$.

We can illustrate the multiplicity suggested by equations (31)–(33) with Fig. 7. Plotted in Fig. 7 are six curves corresponding to $f = 1^\circ, 5^\circ, 10^\circ$ (short-dashed blue curves) and $f = 179.^\circ0, 179.^\circ5, 179.^\circ9$ (long-dashed red curves). We display these curves because they approximate the $e - \Psi$ evolution tracks *beyond* the bifurcation point in the $f \to 0^\circ$ and $f \to 180^\circ$ cases. For these two values of f, $\mathrm{d}f/\mathrm{d}t \approx 0$ (from equation 7), and hence f remains constant as a function of time. In this case, a system will move along one of these tracks. Because Ψ is always increasing, for the blue short-dashed curves, this system will increase its eccentricity until ejection. However, for the red long-dashed curves, the planet's eccentricity might *decrease* until reaching a critical point, when the increase in Ψ will break the constant f approximation and force the system off the track. The critical points (circles; peaks) along these tracks that appear between $1/2 < e \leq 1/\sqrt{2}$, are given by

$$\Psi_{\rm bif,crit1} = \left[-\frac{6\cos f_{\rm bif} + \epsilon}{24\sqrt{3}\sin f_{\rm bif}}\right]\sqrt{5 - 3\cos\left(2f_{\rm bif}\right) - \epsilon\cos f_{\rm bif}}, \tag{34}$$

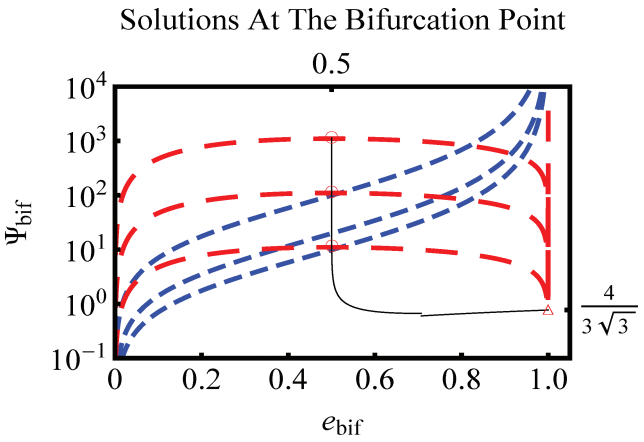

Figure 7. Values of $(\Psi_{\rm bif}, e_{\rm bif}, f_{\rm bif})$ at the bifurcation point, where the blue-short dashed lines, starting from the top down, represent $f_{\rm bif} = 1^\circ, 5^\circ, 10^\circ$, and the red long-dashed lines, starting from the bottom up, represent $f_{\rm bif} = 179\overset{\circ}{.}0, 179\overset{\circ}{.}5, 179\overset{\circ}{.}9$. The peak and trough critical points for the red long-dashed curves are marked with red circles and triangles, respectively. The black curves are given by equations (34) and (35). The blue and red curves, separated by $f_{\rm crit}$ (equation 30), exhibit qualitatively different behaviours. The blue short-dashed curves and the rising portions of the red long-dashed curves represent evolutionary tracks *beyond* the bifurcation point, demonstrating that for $f_{\rm crit} < f < 360^\circ - f_{\rm crit}$, the planet's eccentricity will experience an initial decrease beyond the bifurcation point.

and for those critical points (triangles; troughs) that appear between $1/\sqrt{2} \leq e < 1$:

$$\Psi_{\rm bif,crit2} = \left[-\frac{6\cos f_{\rm bif} + \epsilon}{24\sqrt{3}\sin f_{\rm bif}}\right] \frac{\left(8 - 6\cos^2 f_{\rm bif} + \epsilon\cos f_{\rm bif}\right)^2}{\left(5 - 3\cos\left(2 f_{\rm bif}\right) + \epsilon\cos f_{\rm bif}\right)^{3/2}}, \tag{35}$$

where $\epsilon \equiv \sqrt{18\cos\left(2f\right) - 14}$. The two critical curves are shown in Fig. 7 as thin black lines. The limiting values represented by the three triangles, which are not distinguishable by eye from one another in the plot, occur at $e_{\rm bif} < 1$.

Linking the orbital parameters at the bifurcation point with the initial system orbital parameters is difficult because although the bifurcation point is well defined, the adiabatic approximations begin to break down before the bifurcation point is reached (see, e.g. Fig. 3). Nevertheless, we can analytically estimate the semimajor axis at the bifurcation point by using the semimajor axis adiabat. Doing so gives

$$\begin{aligned}\frac{a_{\rm bif}}{a_0} &= \Psi_0^{-(1/3)} \left[\frac{e_{\rm bif}^{1/3}\left(1 + e_{\rm bif}\cos f_{\rm bif}\right)^{2/3}}{\left(1 - e_{\rm bif}^2\right)^{1/2}\left(\sin f_{\rm bif}\right)^{1/3}}\right] \\ &\propto M_\star^{1/2} a_0^{-(1/2)} \alpha^{-(1/3)}.\end{aligned} \tag{36}$$

Equation (36) contains qualitative physics useful for understanding when the system reaches the bifurcation point. The dependence on the initial stellar mass, initial semimajor axis and the mass-loss rate determines how prone a star is to reaching the bifurcation point and ejecting its planet. For two planets in separate systems with the same a_0, the parent star whose physical parameters yield a smaller value of $a_{\rm bif}$ is more likely to cause ejection. Also, wide-orbit planets are more prone to be ejected than smaller orbit planets. Unfortunately, the term in square brackets is unknown and cannot be bound without some assumptions on $e_{\rm bif}$ and $f_{\rm bif}$. To be consistent with using the adiabat, one can assume $e_{\rm bif} = e_0$. However, by the time the system has reached the bifurcation point, the eccentricity could have already varied away from its initial value by at least a 10th. The value of $f_{\rm bif}$ is the cause of greater uncertainty.

2.6 'Runaway' regime evolution

2.6.1 Runaway true anomaly evolution

The unknown value of $f_{\rm bif}$ largely determines how the planet will evolve past the bifurcation point. If the mass-loss is great and sudden enough, then the planet will bypass the bifurcation point altogether and immediately start evolving in the runaway regime. In this case, the planet's f_0 value is crucial to its evolution. The divided phase-space structure of Fig. 7 correctly suggests that systems can behave quantitatively differently depending on their true anomalies.

Consider Figs 8 and 9, which illustrate the eccentricity evolution as a function of initial true anomaly for $\Psi_0 = 0.089$ (approaching the bifurcation point) and $\Psi = 7.96$ (runaway regime). This dependence is more complex around the bifurcation point $\Psi \sim 0.1$–1 than after it ($\Psi > \Psi_{\rm bif}$). Note importantly that the divided phase-space structure in Fig. 7 manifests itself strongly in Fig. 9 (at $f_{\rm crit}$ in the runaway regime, highlighted by the dotted blue box, when every planet's eccentricity must experience an initial decrease), but not in Fig. 8 (before the bifurcation point). Additionally, in Fig. 8, for at least a third of all the possible initial f_0 values, the first planet ejected has a e_0 value in between the extremes sampled of 0.01 and 0.9. Contrastingly, in Fig. 9, in every instance the first planet ejected has either $e_0 = 0.01$ or 0.9. Further, the eccentricity evolution is nearly symmetric about $f = 180^\circ$ in the runaway regime, a tendency not exhibited in Fig. 8. This helps us to demonstrate how complex the evolution can be when the system is neither robustly in the adiabatic nor in the runaway regime. Planets that have already begun their post-main-sequence life in the strongly runaway regime ($\Psi \gg 1$; Fig. 9) show a more predictable behaviour.

Fortunately, in some cases we can analytically approximate the evolution of orbital parameters in this regime. If a planet begins to evolve at $t = 0$ in a $\Psi \gg 1$ system with a value of f that is close to either 0° or 180°, then f is guaranteed to librate with a small enough amplitude so that f may be treated as a constant. Figs 7 and 9 suggest that the resulting behaviour in each of the two cases will differ qualitatively. The latter figure illustrates that for $f = 180^\circ$, immediately after circularization, the eccentricity evolution starts increasing and continues to do so up until ejection. Before quantifying this behaviour analytically, we attempt to explain the physical mechanism at work.

At $f \approx 0^\circ$, e will increase until the planet is ejected. There is no alternative evolutionary track. At $f \approx 180^\circ$, the eccentricity will decrease until $e \to 0$. In this limit, $|{\rm d}\varpi/{\rm d}t|$ becomes large, forcing ${\rm d}f/{\rm d}t \neq 0$. The true anomaly will then quickly sample other values. At all other values except 0°, ${\rm d}f/{\rm d}t \neq 0$. When f eventually samples 0°, it becomes stuck on that evolutionary track.

2.6.2 Runaway eccentricity evolution

In the runaway regime, when $f = 0^\circ$ or 180°, equations (3) and (4) may be solved directly and analytically. The eccentricity evolution is then given by

$$\begin{aligned}e_{\rm runaway}|_{f=0^\circ} &= e_0\left(1 - \frac{\alpha t}{\mu_0}\right)^{-1} + \left(\frac{\mu_0}{\alpha t} - 1\right)^{-1} \\ &= e_0\frac{\mu_0}{\mu} + \left(\frac{\mu_0}{\mu} - 1\right)\end{aligned} \tag{37}$$

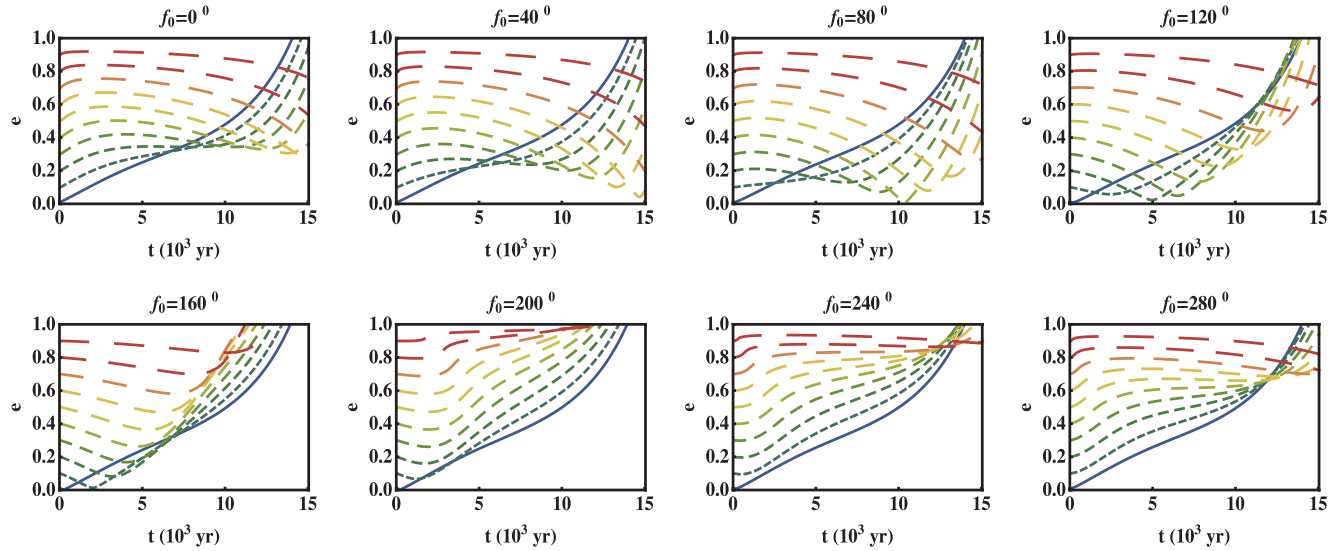

Figure 8. How true anomaly affects eccentricity evolution on the approach to the runaway regime. Shown is the eccentricity of a planet at $a_0 = 500$ au over 1.5×10^4 yr orbiting the same star ($\mu_0 = 1\,\mathrm{M}_\odot$ and $\alpha = 5 \times 10^{-5}\,\mathrm{M}_\odot\,\mathrm{yr}^{-1}$, so $\Psi_0 \approx 0.089$) as in the left-hand panels of Figs 3 and 4, as a function of f_0. The lines with increasing dash length represent e_0 values of 0.01, 0.1, 0.2, 0.3, 0.4, 0.5, 0.6, 0.7, 0.8 and 0.9, respectively. Note the dramatic sensitivity the initial true anomaly may have on the eccentricity evolution, and that for $f_0 = 120°$–$240°$, the particle or planet which is ejected first is one with an initial eccentricity that is neither the highest nor the lowest sampled. The evolution is not symmetric about $f_0 = 180°$, and a few of the initially eccentric planets will become circularized.

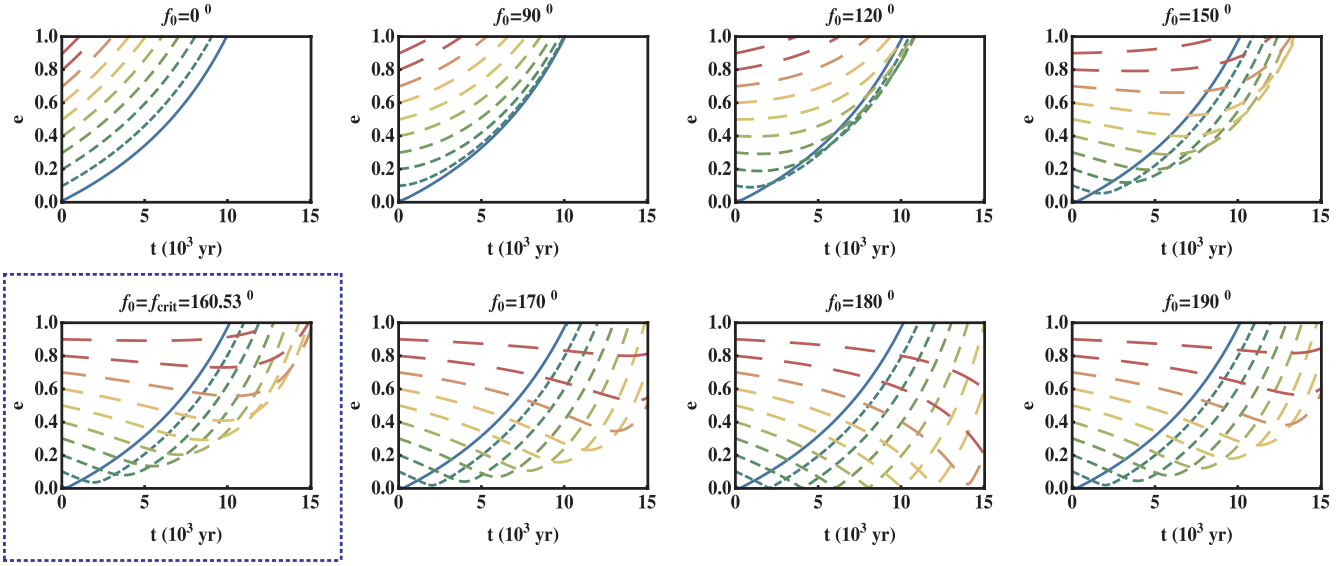

Figure 9. How true anomaly affects eccentricity evolution in the runaway regime. Shown is the eccentricity of a planet at $a_0 = 10^4$ au for the situation in Fig. 8. Here, however, $\Psi_0 \approx 7.96$ and the eccentricity evolution is nearly symmetric about $f_0 = 180°$ (as hinted at by the $f_0 = 170°$ and $190°$ cases). Circular orbits are approached at $f_0 = 180°$. The blue dashed box highlights the case $f_0 = f_{\rm crit}$. For $f_{\rm crit} < f_0 < 360° - f_{\rm crit}$, *every* planet, regardless of e_0, is predicted to experience an initial eccentricity decrease. The eccentricity will later increase if the mass-loss continues for a long enough time (which is not the case, e.g. for $f_0 = 180°$ and $e_0 = 0.8$).

and

$$e_{\rm runaway}|_{f=180°} = e_0 \left(1 - \frac{\alpha t}{\mu_0}\right)^{-1} - \left(\frac{\mu_0}{\alpha t} - 1\right)^{-1} = e_0 \frac{\mu_0}{\mu} - \left(\frac{\mu_0}{\mu} - 1\right). \quad (38)$$

In the $f_0 = 0°$ case, the eccentricity will increase until the planet is ejected; in the $f_0 = 180°$ case, the eccentricity will decrease until the planet achieves a circular orbit. Hence, the amount of mass remaining in a star at the moment of ejection, $\mu_{\rm out}$, and at circulation, $\mu_{\rm circ}$, are

$$\frac{\mu_{\rm out}}{\mu_0} = \frac{1 + e_0}{2}, \quad (39)$$

$$\frac{\mu_{\rm circ}}{\mu_0} = 1 - e_0. \quad (40)$$

Equation (39) demonstrates that for $\Psi > \Psi_{\rm bif}$ and $f_0 \approx 0°$, a planet will be ejected *before half of the star's mass is lost*. Also, planets

with larger initial eccentricities would be the first to be ejected. Equation (40) demonstrates that a planet of any eccentricity may be circularized, and that nearly initially circular planets are the most likely to do so first. These equations may also be expressed as $t_{\rm out} = \mu_0(1-e_0)/(2\alpha)$ and $t_{\rm circ} = \mu_0 e_0/\alpha$.

After circularization, the planet's true anomaly quickly becomes 0°, as described in the last subsection. Then, the eccentricity evolves according to a 'post-circular' prescription:

$$e_{\text{post-circular}} = \frac{t - \frac{\mu_0 e_0}{\alpha}}{\frac{\mu_0}{\alpha} - t} = \frac{\mu_0}{\mu}(1-e_0) - 1. \tag{41}$$

The total time taken for a planet to circularize *and then* be ejected from a system is $t_{\rm tot} = \mu_0(1+e_0)/(2\alpha)$. After this time, the amount of material the star has depleted is

$$\frac{\mu_{\rm tot}}{\mu_0} = \frac{1-e_0}{2}. \tag{42}$$

Any planet that circularizes before becoming ejected therefore must have a parent star that loses *at least half of its mass*. Additionally, in order for the most eccentric planets to be ejected, they require the star to *lose all of its mass*. The implications are that no belt of objects that are uniformly distributed in both true anomaly and eccentricity can all be ejected due to mass-loss: Regardless of the value of Ψ, the highest eccentricity bodies at $f \approx 180°$ must survive.

2.6.3 *Runaway semimajor axis evolution*

The semimajor axis evolution in the $f_0 = 0°$ runaway regime and that in the $f = 180°$ runaway regime are

$$\begin{aligned} a_{\text{runaway}}|_{f=0°} &= a_0(1-e_0)\frac{1-\frac{\alpha t}{\mu_0}}{(1-e_0)-\frac{2\alpha t}{\mu_0}} \\ &= \frac{a_0(1-e_0)}{2-\frac{\mu_0}{\mu}(1+e_0)} \end{aligned} \tag{43}$$

and

$$\begin{aligned} a_{\text{runaway}}|_{f=180°} &= a_0(1+e_0)\frac{1-\frac{\alpha t}{\mu_0}}{(1+e_0)-\frac{2\alpha t}{\mu_0}} \\ &= \frac{a_0(1+e_0)}{2-\frac{\mu_0}{\mu}(1-e_0)}, \end{aligned} \tag{44}$$

respectively. As one might expect, for initially circular orbits in the runaway regime, the semimajor axis evolution is the same for $f_0 = 0°$ and 180°. Also, in the circular limit, we can compare the semimajor axis evolution with what it would have been in the adiabatic limit. For a given a_0, $a_{\text{runaway}}/a_{\text{adiabatic}} = (2\mu/\mu_0 - 1)^{-1}$, which holds until $\mu = \mu_0/2$, the moment the planet is ejected.

Similarly, using equations (39) and (40), one can show that $a_{\rm out} = \infty$ and $a_{\rm circ} = a_0(1+e_0)$. Therefore, the circularization semimajor axis is at most twice the initial semimajor axis. When a planet is circularized, it is done so only momentarily; it can only retain such an orbit if the mass-loss is suddenly stopped at that moment. For any planet that has been circularized, one can show that the semimajor axis will subsequently evolve as

$$a_{\text{post-circular}} = a_{\text{runaway}}|_{f=180°}. \tag{45}$$

Therefore, the semimajor axis evolves through the $e = 0$ transition smoothly, without changing its functional form.

We test the goodness of these analytical approximations by considering a close-in planet (at $a_0 = 2$ au) in the robustly runaway regime of a supernova. Consider a $10\,{\rm M}_\odot$ progenitor that expels $\alpha = 0.5\,{\rm M}_\odot\,{\rm h}^{-1}$ of mass past the orbit the planet. Thus, $\Psi \approx 62.4$. When $f_0 = 0°$ and 180°, equations (37), (38) and (41) replicate the eccentricity evolution. Therefore, we set $f_0 = 20°$ in Fig. 10 to show the extent of the deviation from the analytic approximation. In the figure, the thin black dashed lines represent the analytic approximation, which mimics the true eccentricity evolution to within 10 per cent for all values of e_0. As predicted by equation (39), all planets are ejected before the star loses half of its mass (at 10 h). In Fig. 11, we set $f_0 = 178°$, just 2° off an exact match, because such a deviation from the analytics is more drastic than for deviations of $f_0 = 0°$. As f_0 deviates from 180°, the eccentricity turns up sooner, and becomes less circularized. The approximation will mimic the semimajor axis evolution until the point at which the planet would have been circularized had $f_0 = 180°$. Note that these circularization instances occur when a is less than twice its initial value, in conformity with $a_{\rm circ} = a_0(1+e_0)$. The dots in the left-hand panel indicate when this circularization would have taken place, and show that the semimajor axis evolution is unaffected. As predicted by equation (42), no planets are ejected until at least half

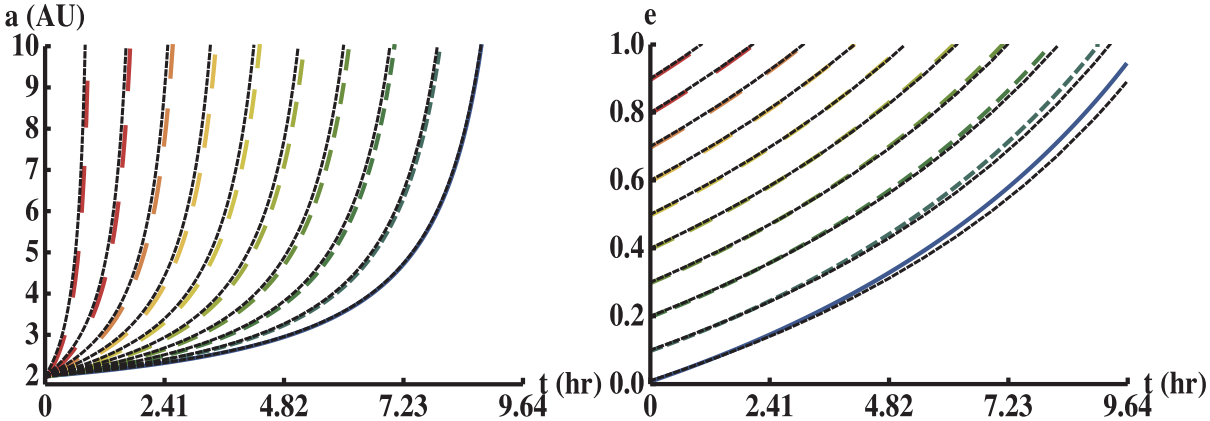

Figure 10. Analytic approximations (thick black nearly solid foreground lines, from equations 37 and 43) to the e and a evolution from the numerical simulations (background-coloured dashed curves) in a robustly runaway regime for $f_0 = 20°$. The planet at $a_0 = 2$ au is experiencing supernova-like mass-loss of $\alpha = 0.5\,{\rm M}_\odot\,{\rm h}^{-1}$ from a $\mu_0 = 10\,{\rm M}_\odot$ star ($\Psi_0 \approx 62.4$). The lines with increasing dash length represent e_0 values of 0.01, 0.1, 0.2, 0.3, 0.4, 0.5, 0.6, 0.7, 0.8 and 0.9, respectively. The analytical approximation is best for $e_0 = 0.01$, and reproduces all the e_0 curves from the full numerical integrations to within 10 per cent. All the planets are ejected before half of the star's mass is lost (see equation 39).

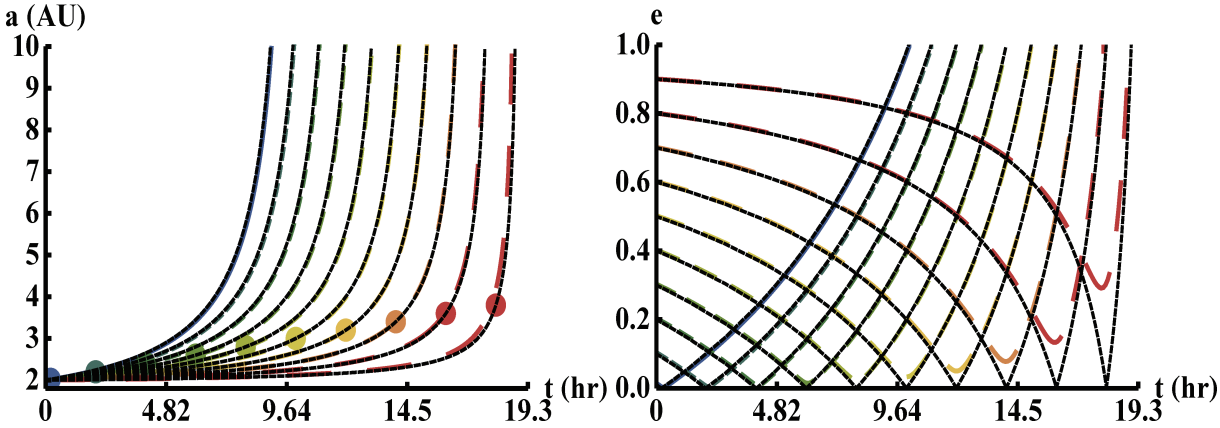

Figure 11. Analytic approximations (thin black nearly solid foreground lines, from equations 38, 41 and 44) to the e and a evolution from the numerical simulations (background-coloured dashed curves) in the same runaway regime as in Fig. 10, but for $f_0 = 178^\circ$. In the limiting case of $f_0 = 180^\circ$, the eccentricity decreases until reaching zero. The dots in the left-hand panel indicate when this would have occurred (at $a_0[1 + e_0]$). None of the planets is ejected until at least half of the star's mass is lost, and the highest eccentricity planets are not ejected until almost all of the star's mass is lost (see equation 42).

of the star's mass is lost, and the highest eccentricity planets are ejected only in the limit of the star losing all of its mass (at 20 h).

2.7 Impulsive regime evolution

One may treat the entirety of stellar mass-loss under the impulse approximation, when the mass is lost instantaneously. This situation corresponds to $\Psi_0 \to \infty$, an asymptotic runaway regime. Let the subscripts 'i' and 'f' represent the initial and final values, $\mathcal{E}$ the (unconserved) specific energy of the system, and r and v the position and velocity of the planet. Then

$$\mathcal{E}_\mathrm{i} = \frac{1}{2}v_\mathrm{i}^2 - \frac{G\mu_\mathrm{i}}{r_\mathrm{i}} = -\frac{G\mu_\mathrm{i}}{2a_\mathrm{o}} \tag{46}$$

and

$$\mathcal{E}_\mathrm{f} = \frac{1}{2}v_\mathrm{f}^2 - \frac{G\mu_\mathrm{f}}{r_\mathrm{f}} > 0, \tag{47}$$

assuming that the planet is ejected.

Now assume $\mu_\mathrm{f} = \beta\mu_\mathrm{i}$, where $0 < \beta \leq 1$. We can obtain a condition for ejection by eliminating $v_\mathrm{i} = v_\mathrm{f}$ from the equations and setting $r_\mathrm{i} = r_\mathrm{f}$. Doing so gives

$$\beta > \frac{1 + e_0^2 + 2e_0\cos f_0}{2\,(1 + e_0\cos f_0)}. \tag{48}$$

We illustrate the phase space suggested by equation (48) in Fig. 12. Below each curve of a given e_0, the planet is ejected. Note how the region around $f_0 = 180^\circ$ highlights a stable region, one for which the highest eccentricity planets are the most protected. This situation is reflected in the finite Ψ runaway regime, and demonstrated in Figs 9 and 11. Although the highest eccentricity planets are the most protected at $f_0 \approx 180^\circ$ (apocentre), they are the least protected at $f_0 \approx 0^\circ$ (pericentre). The tendency for nearly circular planets to be ejected is independent of true anomaly.

One curious connection between the impulse approximation and the bifurcation point is that the two inflection points of equation (48) satisfy equation (23). The value of β at these points, β_infl, is given by

$$\beta_\mathrm{infl} = \frac{1}{8}\left(5 - \sqrt{1 + 8e_0^2}\right). \tag{49}$$

Therefore, $1/4 \leq \beta_\mathrm{infl} \leq 1/2$. These points are marked as dots in Fig. 12, and are connected by the analytic curve from equations (23) and (49).

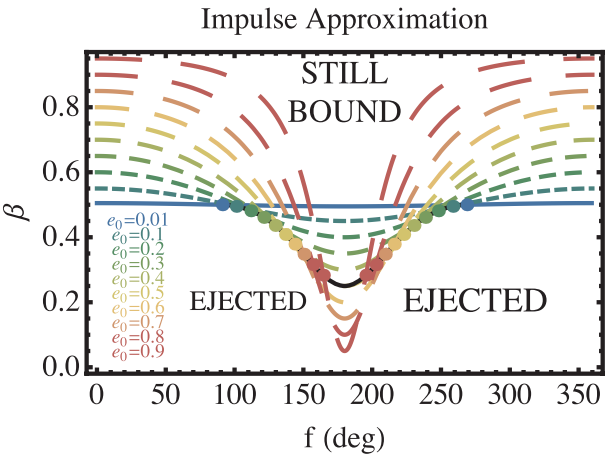

Figure 12. Ejection prospects in the impulse approximation ($\Psi_0 \to \infty$). Plotted is the fraction of stellar mass retained ($\equiv \beta$) versus f_0 for 10 curves of increasing dash length for $e_0 = (0.01, 0.1, 0.2, 0.3, 0.4, 0.5, 0.6, 0.7, 0.8, 0.9)$. The planet remains bound in the regions above the curves and is ejected in the regions below the curves. The dots refer to the inflection points of the curves, given by equation (49) and which satisfy equation (23). Note how highly eccentric planets are especially protected from ejection near apocentre ($f \approx 180^\circ$), but are prone to ejection near pericentre ($f \approx 0^\circ$).

Returning to equation (48), note that in the limits of $f \to 0^\circ$ and $f \to 180^\circ$, one recovers equations (39) and (42). Additionally, if the inequality in equation (48) is solved for $\cos f$ and then bounded by its maximum value, then ejection is impossible if

$$\beta > \frac{1 + e_0}{2}. \tag{50}$$

This condition demonstrates that for an initially circular planet, at least half of the star's mass must be lost in order for there to be a possibility of ejection. For a highly eccentric planet, however, just a slight mass-loss might be enough to eject it. Whether or not a planet's high eccentricity serves as a protection mechanism is dependent on its f value, which relates how close the planet is to the pericentre or the apocentre.

As an example, consider a circular ring of massless particles uniformly distributed in true anomaly at any separation from a star of any non-zero mass. If over half of the star's mass is lost instan-

taneously, then the entire particle ring will be ejected. Otherwise, all the particles will remain bound. Now consider an eccentric ring where all particles have $e = 0.9$. If the parent star instantaneously loses 60 per cent of its mass, then only ≈11 per cent of the ring will remain bound to the star.

3 EXCITATION AND EJECTION IN REALISTIC SYSTEMS

3.1 Overview

We can now apply the theory developed in Section 2 to realistic systems. The field of stellar evolution is extensive and touches on several areas of astrophysics. We cannot hope to cover the entire phase space in detail in one paper. However, by focusing on a single phase of stellar evolution and considering constant mass-loss in most cases, we will attempt to provide preliminary statistics and an order-of-magnitude analysis for the entire progenitor stellar mass range up to $150\,\mathrm{M}_\odot$. We perform detailed non-linear simulations only for the $2\,\mathrm{M}_\odot \leq \mu_0 \lesssim 7\,\mathrm{M}_\odot$ regime, whose stellar evolutionary tracks lend themselves well to this study.

The evolution of stars is almost entirely determined by its ZAMS (zero-age main sequence) metallicity content and mass (Woosley, Heger & Weaver 2002). These two factors determine how mass is lost later in life through winds. Because this correlation is so poorly known, mass-loss prescriptions are often treated as a third independent parameter for tracing stellar evolution. To avoid detailed modelling involving integration of the stellar evolution differential equations, we rely heavily on the empirical algebraic fits of Hurley, Pols & Tout (2000) to model the evolutionary tracks of stars of most mass, metallicity and mass-loss rate properties. These evolutionary tracks demonstrate that mass-loss (i) can occur in multiple stellar phases, (ii) is often prominent in just one stellar phase, and (iii) is always monotonic but typically non-linear in any given phase. All the stellar evolutionary phase names used here are defined in their seminal work.

We use the mass-loss prescriptions provided in Hurley et al. (2000), which include the Reimers law on the red giant branch (RGB; Kudritzki & Reimers 1978), a steady superwind asymptotic giant branch prescription (Vassiliadis & Wood 1993), a high-mass-loss prescription (Nieuwenhuijzen & de Jager 1990), a Wolf–Rayet-like mass-loss prescription (Hamann, Koesterke & Wessolowski 1995) and a luminous blue variable law (Humphreys & Davidson 1994). The Reimers prescription is in particular widely used for giant branch evolution, and beyond:

$$\frac{\mathrm{d}M_\star}{\mathrm{d}t} = \eta\left(4\times10^{-13}\right)\frac{L_\star(t)\mathcal{R}_\star(t)}{M_\star}\frac{\mathrm{M}_\odot}{\mathrm{yr}}, \tag{51}$$

where $L_\star$ and $\mathcal{R}_\star$ are the stellar luminosity and radius and η is a dimensionless coefficient. We adopt the 'typical' value for η of 0.5 (Hurley et al. 2000; Schröder & Cuntz 2005).

We divide the stellar mass phase space into five regimes, which are approximately separated at 1, 2, 7 and $20\,\mathrm{M}_\odot$, based on stellar evolutionary properties.

3.2 Numerics and checks

Although certain regimes of evolution can be modelled well by algebraic formulas, the lack of a complete closed-form analytical solution to equations (3)–(7) suggests that numerical integrations are needed to model the evolution of the full two-body problem with mass-loss. We evolve planetary orbits in this section by using numerical integrations.

In these integrations, one may incorporate mass-loss (i) as a separate differential equation, (ii) by explicitly removing mass from the primary according to a given prescription, or, alternatively (iii) by adding mass to the secondary (Debes & Sigurdsson 2002). As a check on our results, we have reproduced each curve in the breaking of adiabaticity regime in the left-hand panel of Fig. 3 ($\Psi_0 \approx 0.023$) with both (i) integration of the orbital elements (equations 3–7) plus integration of a separate mass-loss differential equation in the MATHEMATICA software program, for 13 digits of accuracy and precision and with a working precision equal to machine precision, and (ii) integration of the Cartesian equations of motion with the hybrid integrator of the N-body code, *Mercury* (Chambers 1999), with a maximum time-step of 1 yr and with mass explicitly being removed from the primary at each time-step.

However, we warn future investigators that in systems that ultimately do not obey the adiabatic approximation, the dynamical evolution is sensitive to the evolution of f. Therefore, in numerical integrations, particularly for non-linear mass-loss prescriptions, how one discretizes the continuous mass-loss process can qualitatively affect the resulting evolution. A discretation of mass-loss is mimicked in reality by instantaneous bursts of primary mass lost beyond the orbit of the secondary. Therefore, a detailed study of an individual system with a given mass-loss prescription will require a numerical integration where the time between discrete decreases in the primary mass should be less than the (largely unknown) time-span of discontinuous patterns in the mass-loss modelled. Here, we just seek to demonstrate the instability in the general two-body mass-loss problem and achieve representative statistics on ensembles of systems. In the $2\,\mathrm{M}_\odot \leq \mu_0 \lesssim 7\,\mathrm{M}_\odot$ regime, which features non-linear mass-loss, we model planets with $50\,\mathrm{au} \leq a_0 \leq 10^5\,\mathrm{au}$. Therefore, we set a maximum possible time-span of 1 yr (the same value used to reproduce Fig. 3) between mass lost; in order to achieve mass-loss on this scale, we interpolate linearly between the outputs from the largely non-linear stellar evolutionary track outputs from Hurley et al. (2000). We then run the simulations with *Mercury's* (Chambers 1999) hybrid integrator.

3.3 The stellar mass spectrum

3.3.1 The $\mu_0 < 1\,M_\odot$ regime

Subsolar-mass stars experience quiescent deaths, some of which are theorized to last longer than the age of the Universe. However, stellar tracks computed from the Hurley et al. (2000) code indicate that the most massive members of this group ($\mu_0 > 0.7\,\mathrm{M}_\odot$) may pass through multiple stages of evolution, and eject up to half of their initial mass in the RGB stage. Low-metallicity $\mu_0 = 0.8$ and $0.9\,\mathrm{M}_\odot$ stars do so on the RGB over ∼100–200 Myr. If this mass is lost uniformly, then $\Psi_0 \approx 0.011$, meaning that the system is likely to start losing its adiabatic properties. Simulations of *constant* mass-loss confirm that the change in the eccentricity of an Oort Cloud at $a_0 = 10^5$ au will vary from ∼0.01 (for particles with $e_0 = 0.90$) to ∼0.1 (for particles with $e_0 = 0.01$). The mass-loss is not strong and quick enough to eject the particles, and objects with semimajor axis less than $\sim10^4$ au (which would yield $\Psi \leq 0.00036$) are robustly in the adiabatic regime. This regime of the motion might change, however, due to non-linear modelling. This might reveal short bursts of mass-loss causing Ψ to increase sharply over the corresponding burst time-scale.

3.3.2 The $1 \leq \mu_0 < 2\,M_\odot$ regime

Roughly half of all known planet-hosting stars, including the Sun, lie in this progenitor mass regime, motivating detailed analyses of these systems. We defer such analyses to future studies because of the complex multiphasic evolutionary path these stars are prone to follow.

As an example, assuming $\eta = 0.5$, the Sun will eventually lose a total of 48 per cent of its original mass: 24 per cent during RGB, 4 per cent during core-He burning, 13 per cent during early asymptotic giant branch (EAGB), and 7 per cent during thermally pulsing asymptotic giant branch (TPAGB). All these phases of mass-loss are non-linear and occur on different time-scales. If instead $\eta = 0.3$, then the mass-loss percentages will change drastically: 13 per cent during RGB, 2 per cent during core-He burning, 4 per cent during EAGB, and 28 per cent during TPAGB. Other examples show that slightly increasing the progenitor mass from 1.1 to 1.2 $M_\odot$ can have a similarly large effect on what mass is lost when.

We can, however, provide some rough estimates of planetary evolution through representative numerical simulations assuming constant mass-loss over one phase. Stars in this mass regime may lose over 60 per cent of their original mass, most of which either in RGB (particularly for values of $\eta \geq 0.8$) or TPAGB (for lower η and $\mu_0 > 1.3\,M_\odot$). The duration of RGB phases for these masses are $\sim$100 Myr, and will yield only minor eccentricity increases at $a = 10^5$ similar to those from subsolar masses. However, the duration of TPAGB phases in this mass regime is $\sim$0.1–1.0 Myr. Constant mass-loss over this period of time for $\mu_0 = 1.0$–$1.3\,M_\odot$ can cause up to 20 per cent of an Oort Cloud at 10^5 au ($\Psi \approx 3.0$) to be ejected, and raise the eccentricity of an initially circular planet at 10^4 au ($\Psi \approx 0.096$) to $\approx$0.25. We obtained these figures by sampling eight evenly spaced values of f_0 for each of the following 10 values of e_0: 0.01, 0.1, 0.2, 0.3, 0.4, 0.5, 0.6, 0.7, 0.8, 0.9. This effect is pronounced with progenitor masses approaching 2 $M_\odot$ and losing up to 70 per cent of their initial mass.

Therefore, Oort Clouds are in jeopardy of partially escaping or being moderately disrupted in systems with similar progenitor masses to the Sun. The comets cannot, however, drift into the inner regions of the system (see equation 21). The widest orbit planets at $\sim 10^4$ au may experience a moderate eccentricity change of a few tenths, and might be ejected depending on the non-linear character of the mass-loss. Future multiphasic non-linear modelling will better quantify and constrain these effects.

3.3.3 The $2 \leq \mu_0 \lesssim 7\,M_\odot$ regime

This mass regime is well suited for this study because here, $\sim$70–100 per cent of a star's mass-loss occurs in a single phase, the TPAGB, regardless of the values of η, [Fe/H], or μ_0. Therefore, by modelling the non-linear mass-loss in this one phase, we can make definitive conclusions about this region of phase space. Additionally, the duration of this phase is short, typically under 2 Myr, and therefore feasible for numerical integration of planets at distances of just a few tens of au.

We consider two progenitor star metallicities, a 'low' metallicity ([Fe/H] = 0.0001) and a solar metallicity ([Fe/H] = $[\mathrm{Fe/H}]_\odot$ = 0.02), both with $\eta = 0.5$. In the low-metallicity case, we utilize nine TPAGB evolutionary tracks in the range of $\mu_0 = 2$–$6\,M_\odot$, in increments of 0.5 $M_\odot$. In the solar metallicity case, we utilize 13 TPAGB evolutionary tracks in the range of $\mu_0 = 2$–$8\,M_\odot$, in increments of 0.5 $M_\odot$. Beyond these upper mass limits, a star would undergo the supernova stage for the stated metallicities. The evolutionary tracks are plotted in Fig. 13. Note that the initial masses indicated on the plots do not exactly represent μ_0; the small (<10 per cent) mass-loss that occurred between the main sequence and the start of the TPAGB, typically in the core-He burning and EAGB phases, has already been subtracted. For all of the tracks except the low-metallicity $\mu_0 = 2\,M_\odot$ track, most of the mass-loss occurs within a short 10^4 yr scale indicated by the sharp downturn in the curves. However, note that between the start of the TPAGB phase to this intense mass-loss period, over a period of $\approx$0.7–1.5 Myr, the stars typically lose $\sim$0.5 $M_\odot$ worth of mass. After the intense mass-loss burst, effectively no more mass is lost from the system. Integrations for the two lowest mass tracks for [Fe/H] = $[\mathrm{Fe/H}]_\odot$ = 0.02 were begun 5×10^5 yr after the start of the TPAGB in order to include the sharp mass-loss feature and consistently integrate all systems over the same period of time.

For each of the 22 evolutionary tracks, we modelled 1200 planets as test particles and integrated the systems for 1.6 Myr, longer than the duration of the TPAGB phase for nearly all of the stellar tracks. The planets were all given randomly chosen values of the initial mean anomaly, and were split into eight groups of 150 each. Each group of planets was assigned an a_0 value of 50, 100, 500, 1×10^3, 5×10^3, 1×10^4, 5×10^4, and 1×10^5 au. Each group of 150 planets was split into three subgroups of 50, each of which was assigned an e_0 value of 0.01, 0.5 and 0.9.

We compute the percentage of each group of 150 simulations of a given semimajor axis and initial progenitor mass that become

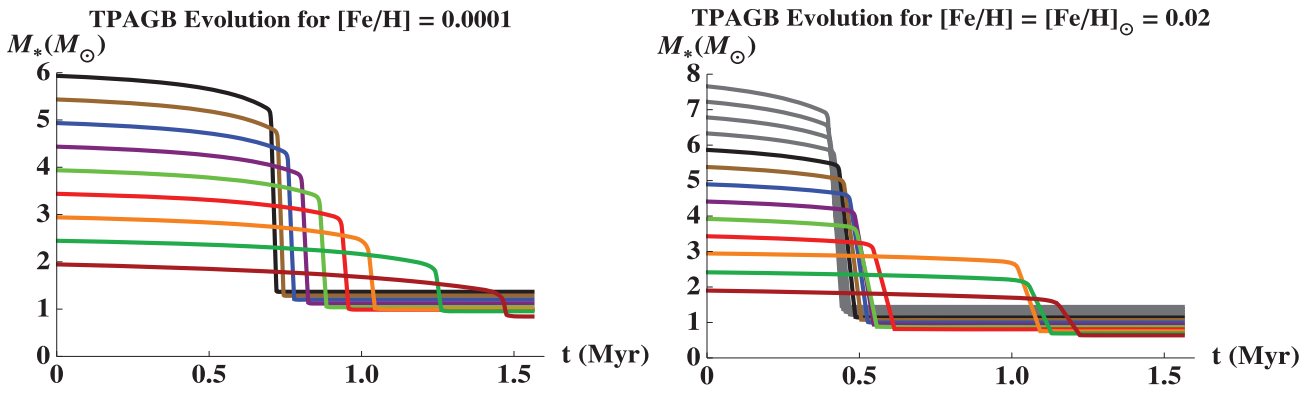

Figure 13. Thermally pulsing asymptotic giant branch (TPAGB) evolution for stars of low- and solar-metallicities. Each colour represents a different evolutionary track. Initial TPAGB mass can be read off from the Y-axis. The four highest mass grey curves for solar metallicities were not computed for the low-metallicity case because those stars would have undergone the supernova stage.

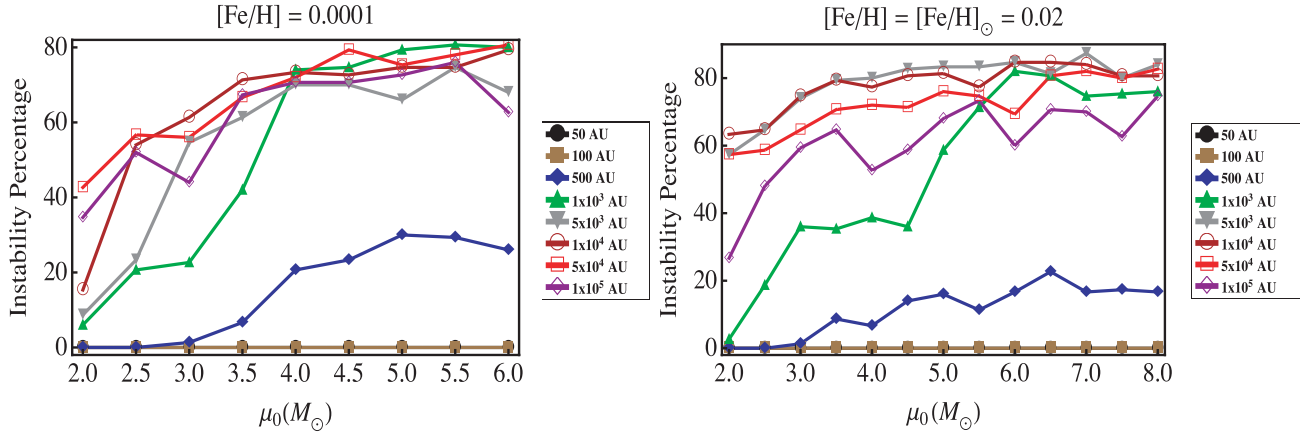

Figure 14. Planetary ejection prospects for massive stars at 2–8 $M_\odot$. Each data point is averaged over the 150 randomly chosen mean anomaly values and three selected e_0 values for each a_0. The black filled-circle curves for 50 au are hidden behind the 100 au curves. The $a_0 = 50$ and 100 au systems, which are in the adiabatic regime, remain bound. The $a_0 \geq 10^3$ au systems, in the runaway regime, become largely unstable.

unstable. We define instability by whether or not the planetary eccentricity reaches unity. Fig. 14 reports the results. Because of the non-linear nature of the mass-loss, here our mass-loss index from equation (15) breaks down. However, we can say roughly that the duration of the greatest mass-loss is comparable to a planet's period at 500 au (the blue curves with diamonds). At approximately this semimajor axis we expect a planet to be in the transition region between adiabaticity and runaway. These curves on the plot qualitatively corroborate this expectation: orbits tighter than 500 au are stable and adiabatic, orbits wider than 500 au are unstable and runaway, and orbits at 500 au are a bit of both. Most of the planets in the widest orbits become unstable, but they cannot all become unstable for a large enough sample of randomly chosen values of f_0 because some of these values will be close to 180°. As demonstrated by Fig. 11, in the high (e.g. 0.9) e_0 case, planets with f_0 close to 180° will be ejected only if the parent star loses over ∼95 per cent of its mass, a largely unrealistic scenario for any progenitor mass. Further, for the simulations in Fig. 14, note that beyond 1000 au – in the robustly runaway regime – there is little correlation with instability percentage and a_0. Equations (37), (38) and (41) help us to show why: at least for values of f_0 close to 0° and 180°, the eccentricity evolution is *independent of* a_0.

For planets that remain bound, we consider the extent of their eccentricity excitation. Fig. 15 plots the eccentricity range experienced by bound planets averaged over all simulations with the same values of μ_0, a_0 and e_0 but with different values of f_0. The panels show that the eccentricity of the remaining bound planets for $a_0 \geq$ 500 au is significantly excited (by several tenths). The eccentricity of planets at $a_0 = 50$ and 100 au on average can vary by a few hundredths, and 0.1, respectively. If a symbol in the legend does not appear on the corresponding plot, then no planets at that semimajor axis remains bound. The top two panels ($e_0 = 0.01$) exhibit a dearth of these symbols, a result one might expect from Fig. 12. If that figure is qualitatively representative of the situation here, amidst strong non-linear mass-loss, then there is no value of f_0 that affords the lowest e_0 planets protection. The horizontal lines on the middle two and bottom two panels of Fig. 15 display the value of $1 - e_0$; symbols above these lines indicate that the corresponding systems on average experience a net eccentricity decrease. These systems are more likely to be left with a planet whose orbit is less eccentric than e_0 when mass-loss is terminated.

3.3.4 The $7 \lesssim \mu_0 \lesssim 20\,M_\odot$ regime

Generally, solar-metallicity stars with $8 \leq \mu_0 \leq 20\,M_\odot$ are thought to undergo supernova and produce a neutron star. However, these bounds are approximate. Additionally, lower metallicity stars can begin neutron star formation and black hole formation at different values; the representative ones might be 6 and 18 $M_\odot$, respectively (Heger et al. 2003; Eldridge & Tout 2004; Belczynski et al. 2010). These stars may eject ∼50–95 per cent of their initial mass, most of which is in the supernova (Smartt et al. 2009). Additionally, the minimum and maximum possible masses of the remnant neutron stars are constrained by physical principles. Typically accepted values for the minimum and maximum are ≈1 $M_\odot$ (Strobel & Weigel 2001) and 3 $M_\odot$ (Kalogera & Baym 1996); Clark et al. (2002) presents observational evidence for the upper bound. Therefore, this mass regime of stellar evolution is relatively well constrained, and due to the nearly instantaneous mass-loss, is very well suited for this study.

The sudden nature of the formation of a supernova, combined with the great extent of mass lost compared to μ_0, places any orbiting planet immediately in the runaway regime. Therefore, we seek to determine what planets, if any, can *survive* a supernova. We hence choose parameters that favour survival, to see if this situation is possible. First, we select the minimum possible a_0. Evolutionary tracks from Hurley et al. (2000) indicate that the minimum extent of the pre-supernova stellar envelope (including pre-supernova mass-loss) is about ∼2 au, so we choose $a_0 = 2$ au.

If the mass ejected from a supernova is considered to be isotropic, then this mass will collide with any orbiting bodies. This collision is likely to destroy smaller bodies. Large and/or massive planets, however, may survive. Those planets that do survive might accrete some of the mass from the ejecta. Although doing so will cause a to decrease, this contribution, even at 2 au, is negligible compared to the a increase from all the other ejecta that are being blown past the planet's orbit. We are concerned with the amount of time the mass takes to pass the diameter of the planet. We can model mass-loss in these systems by assuming an ejection velocity and a planetary diameter.

Observations help us to constrain the velocity of this ejecta. Some diverse examples for different types of supernovae include the following.

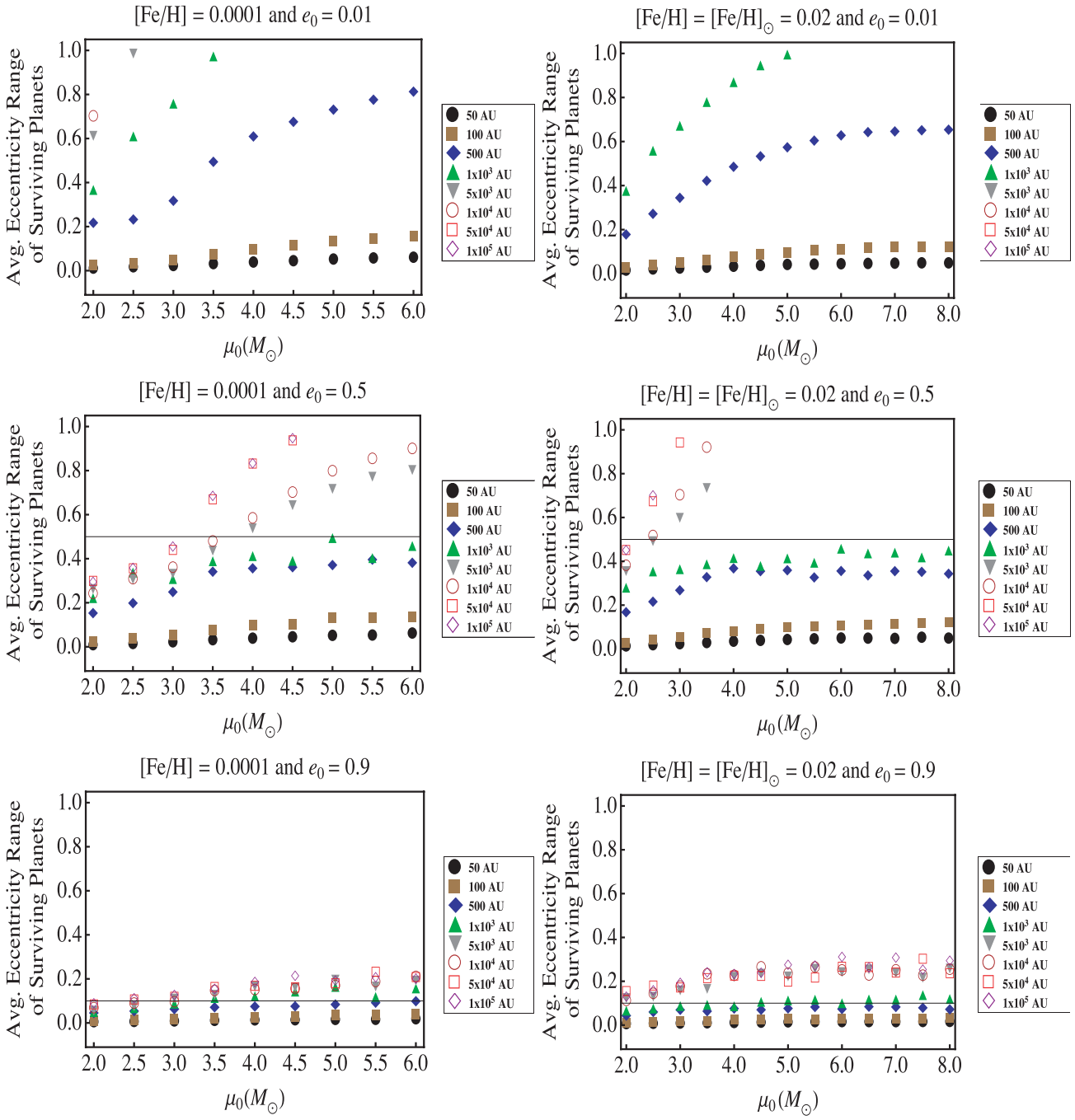

Figure 15. Eccentricity excitation of planets which remain bound during massive star evolution, for 2–8 $M_\odot$. The left- and right-hand panels are for low metallicity and solar metallicity, respectively. The top, middle and bottom panels are for $e_0 = 0.01$, 0.5 and $e = 0.9$, respectively. Each data point is averaged over the 50 values of the mean anomaly sampled for the given μ_0, a_0 and e_0 values. If no symbol is displayed, then none of the corresponding systems was stable. The horizontal lines indicate values of $1 - e_0$; symbols above this line experience a net eccentricity decrease.

(i) Fesen et al. (2007) report *Hubble Space Telescope* observations that indicate that the 120 yr average expansion velocity of SN 1885 is $1.24 \times 10^4 \pm 1.4 \times 10^3$ km s^{-1}.

(ii) Mazzali et al. (2010) model spectra of SN 2007gr, and find that the inner 1 $M_\odot$ of material is being ejected at a velocity of 4.5×10^3 km s^{-1}.

(iii) Szalai et al. (2011) find that the maximum velocity of supernova ejecta of 2004dj during the nebular phase is approximately 3.25×10^3 km s^{-1}.

One theoretical investigation claims that ejecta velocity can reach 2×10^4 to 3×10^4 km s^{-1} (Woosley, Langer & Weaver 1993), and another demonstrates that (surface) piston speeds of 1×10^4–2×10^4 km s^{-1} 'covers the extremes from a sudden (energy deposition over 1 s) to a slow-developing explosion (energy deposition over ~100 ms)' (Dessart, Livne & Waldman 2010). As exemplified by these examples as well as the compilation in fig. 1 of Hamuy & Pinto (2002), a typical range is $v = 10^3$–10^4 km s^{-1}; let us then assume the lower bound $v = 10^3$ km s^{-1}.

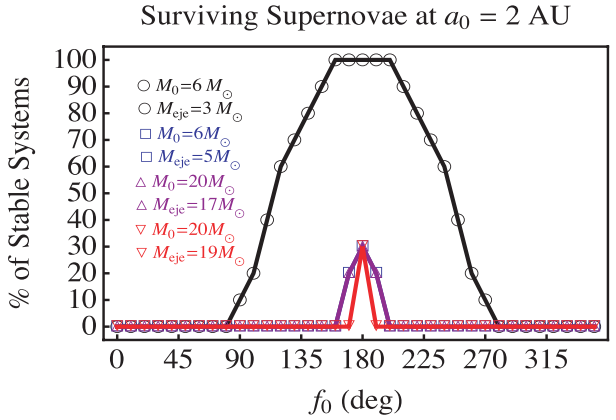

Figure 16. Survivability of a tight-orbit (2 au) planet during supernova. The progenitor mass and ejected mass is given by M_0 and M_{ej}, respectively. Each data point is based on 10 systems with $e_0 = (0.01, 0.1, 0.2, 0.3, 0.4, 0.5, 0.6, 0.7, 0.8, 0.9)$. For all cases, $\Psi_0 \approx$ 1–2. The plot demonstrates that the only way planets may remain bound after a supernova blast is by initially residing in a narrow region of true anomaly space. This behaviour was predicted in Sections 2.6.2 and 2.7, and specifically in Fig. 12. Equation (48) demonstrates why *all* planets on the black curve with open circles with $160^\circ \leq f_0 \leq 200^\circ$ survive, and why *all* planets near pericentre are ejected. Almost all planets that withstand a supernova are ejected unless the percentage of the progenitor's mass lost is the theoretical lower bound ($\approx$50 per cent) for supernovae of $\approx$7–20 $M_\odot$ progenitor masses.

Further, the highest known exoplanet radius is less than twice Jupiter's radius,[3,4] so let us assume this value for our planet. We can then test the extremes of the total mass lost ($\equiv M_{ej}$) based on the progenitor mass and remnant mass bounds.

We assume the mass is blown past the orbit of the planet isotropically and at a constant value, and we consider 36 uniformly distributed values of f_0. For each, we adopt 10 values of e_0 (0.01, 0.1, 0.2, 0.3, 0.4, 0.5, 0.6, 0.7, 0.8, 0.9). We simulate these 360 systems in each of four scenarios: with the two extreme values of μ_0 (6 and 20 $M_\odot$) and two extreme values of the remnant mass (1 and 3 $M_\odot$). For all these cases, $\Psi_0 \approx$ 1–2, placing these systems in the weak runaway regime at $t = 0$. The reason why Ψ_0 is not higher for such a great mass-loss rate is a_0 is so low (2 au). However, to determine the endpoint of orbital evolution, one needs to combine an estimate of Ψ_0 with a mass-loss duration time (or a remnant mass, for constant mass-loss), which is independent of Ψ_0. This is why the end-states can change drastically for two systems even if their initial mass-loss indices are equivalent.

Fig. 16 displays the result of our simulations. The figure demonstrates that an appreciable number of planets *can* survive, but only in the extreme case of the supernova ejecting just half of the progenitor mass, and only if f_0 is closer to 180° than to 0°. In the more realistic cases of a greater mass-loss during supernova, the only planets that may survive must have $f_0 \approx 180^\circ$. This initial condition appears to be the only protection mechanism against ejection for robustly runaway (see Fig. 11) or impulsive (see Fig. 12) systems that lose most of their mass. The impulsive limit can further help us to explain Fig. 16 through equation (48): the top, black curve with open circles corresponds to $\beta = 1/2$, and the highest initial eccentricity we sampled in the simulations was $e_0 = 0.9$. Therefore, equation (48) gives $\cos f_0 < -0.9$, meaning that *all* planets with $154^\circ \lesssim f_0 \lesssim 206^\circ$ should remain stable. The numerical simulations confirm the theory. Additionally, Fig. 12 confirms why no planets with initial true anomalies within 80° of pericentre survive, even when just half of the star's mass is lost.

In fact, if we decrease or increase the mass-loss rate (and hence Ψ_0) by an order of magnitude (to either $v = 100$ or 10^4 km s^{-1}), and rerun our simulations, we reproduce Fig. 16 closely. Therefore, in such runaway regimes, the evolution becomes *independent* of the mass-loss rate above a certain critical mass-loss rate. The realistic implication of this finding is that the particular choice of ejecta velocity assumed for a supernova is unimportant, as long it is assumed to be higher than a critical minimum value.

3.3.5 *The $\mu_0 \gtrsim 20\,M_\odot$ regime*

There is great uncertainty regarding how the highest mass stars lose mass and in what amounts. The possibilities for planetary evolution around these stars are intriguing, and can be simulated once a model has been adopted for a particular star. Stars in this regime generally become neutron stars or black holes.[5] Heger et al. (2003) and Eldridge & Tout (2004) outline these potential stellar fates as a function of initial progenitor mass and metallicity.

Black holes may form with or without a supernova. In the latter case, mass is still lost during core collapse. Quantifying the extent and time-scale of this mass-loss is crucial for determining the fate of any orbiting planets. This process is thought to last on the order of tenths of seconds to seconds (O'Connor & Ott 2011). The mass lost during this process has been modelled to be as much as 1–2 $M_\odot$ (Belczynski et al. 2010). However, this value could be zero; Fryer (1999) argues that for progenitor masses above 40 $M_\odot$, the final black hole mass could be as large as the progenitor. Zhang, Woosley & Heger (2008) indicates that stars at even greater masses, with $100 < \mu_0 < 260\,M_\odot$, may explode completely and leave no remnant. These theoretical treatments are poorly constrained by observations. However, observations do suggest that stars up to 300 $M_\odot$ exist (Crowther et al. 2010).

Hence, unlike in the previous subsections, stellar mass evolution here remains qualitatively uncertain, as the amount of initial mass lost could be any value up to 100 per cent. Therefore, we can frame our cursory analysis in this section by considering what *per cent of the progenitor's mass must be lost* in order to produce ejection or excitation. The large progenitor masses in this regime promote adiabaticity, as indicated by equation (15), and hamper prospects for planetary ejection, as indicated by equation (36). However, mass could be lost through superwinds at a great rate of $10^{-4}\,M_\odot$ yr^{-1} (Dessart et al. 2010; Yoon & Cantiello 2010), which might offset the stabilizing effect of the large magnitude of the progenitor mass.

We can provide a preliminary overview of the impact large progenitor masses with superwinds would have on the survivability of planets. We consider three (strong) mass-loss rates, $\alpha = \{10^{-4}, 10^{-5}, 10^{-6}\}\,M_\odot$ yr^{-1} and progenitor masses up to 150 $M_\odot$. For all these cases, unless $a_0 \gtrsim 10^4$ au, the planetary evolution will be primarily adiabatic, as $\Psi_0 \ll 1$. We find that at least $\sim$80 per cent of a progenitor's mass must be lost for any planet at $a_0 \sim 10^3$ au to be ejected by any of these winds. However, for planets at $a_0 \sim 10^5$ au, a mass-loss of $\alpha = 10^{-4}\,M_\odot$ yr^{-1} does place the planet in a runaway regime. In this regime, for $f_0 = 0^\circ$, the progenitor needs

[3] Extrasolar Planets Encyclopaedia at http://exoplanet.eu/
[4] Exoplanet Data Explorer at http://exoplanets.org/

[5] In rare cases, at the very lowest metallicities, pair instability supernovae will destroy the entire star and leave no stellar remnant.

to lose just a few per cent of its initial mass to eject the highest eccentricity planet, and roughly 50 per cent of its mass to eject initially circular planets. These results conform to expectation from equation (39), and hold for all progenitor masses of 20–150 $M_\odot$. Therefore, even without appealing to core collapse or weak supernova, the mass-loss from the highest mass stars in the Universe can blow away any remaining Oort Clouds.

Detailed modelling of secondaries evolving amidst the complex evolution of stars in this mass regime is a ripe topic for future studies. Although the mass lost in core collapse can approach zero, the nearly instantaneous time-scale for the mass-loss might have a sudden pronounced effect on the planetary orbit. Further, fall-back of mass from a weak supernova explosion on to a neutron star lasting 'seconds to tens of hours' (Heger et al. 2003) could trigger a black hole. This fall-back will cause a still-bound planet's semimajor axis to *decrease*. Also, for stars that explode away almost 100 per cent of their mass, one may investigate the minimum amount of mass that could remain and still bind a planet. In this case, the planet's mass will become important.

4 DISCUSSION

4.1 Oort Clouds

No Oort Clouds have been observed. However, comets thought to originate in the Sun's Oort Cloud have been observed, and have motivated several studies that estimate the orbital extent of these bodies. Levison et al. (2010) claim that the Oort Cloud extends to $\sim 10^5$ au, and Dybczyński (2002) claims that this is a 'typical' value for the outer boundary. Although planetary material might exist throughout the scattered disc from the Kuiper Belt to the Oort Cloud (e.g. Leto et al. 2008), some authors (Duncan, Quinn & Tremaine 1987; Gardner et al. 2011) have set an inner boundary at several thousand au. Other studies focus on a supposed break in the Oort Cloud, separating it into an 'inner' and 'outer' region. This bifurcation is claimed to occur at at $\sim 2 \times 10^4$ au (Hills 1981; Kaib & Quinn 2008; Brasser, Higuchi & Kaib 2010).

These estimates pertain only to the Solar system. Oort Clouds around other stars may exist. Stars born in denser clusters will have more comets deposited into their clouds than did the Sun. Kaib & Quinn (2008) simulate four different primordial environments (with no cluster, and three clusters with densities of 10, 30 and 100 stars per cubic parsec) and find that all produce similar 'outer' ($a > 2 \times 10^4$ au) Oort Clouds and qualitatively different inner ones. Further, Brasser et al. (2010) consider the different types of Oort Clouds that may form around other stars as a function of Galactocentric distance. At large Galactocentric distances (>14 kpc), they find that some (>10 per cent) Oort Cloud constituents orbit beyond 10^5 au.

All these estimates suggest that the majority of stellar mass progenitors, including the Sun and those of subsolar mass, will excite the eccentricity of Oort Clouds during stellar evolution. Most of these Oort Clouds will lose material to interstellar space. Assuming that the comets are roughly distributed uniformly in true anomaly, then only a fraction will survive. This fraction is highly dependent on the duration of mass-loss. The remaining comets will assume a differential eccentricity distribution. Brasser et al. (2010) focus on Galactic tides and how they strip off Oort Cloud constituents. Indeed, Oort Clouds may not even survive to the post-main-sequence phase. If they do, the Galactic tide will be stronger relative to the star's gravity for any surviving Oort Cloud objects, so the stable region that the Oort Cloud can occupy will have shrunk at the same time that the bodies' orbits are expanding, potentially leading to even more ejections. Further, as a star loses mass, its gravitational influence within its stellar neighbourhood will shrink and be encroached by the potential wells of stellar neighbours.

However, as demonstrated by fig. 3 of Higuchi et al. (2007), Galactic tides often need Gyr of evolution in order to cause an appreciable change in a comet's orbital elements. Short-lived massive stars will not often provide Galactic tides with this opportunity before stellar mass-loss becomes the dominant perturbation on the comets.

A more detailed modelling of Oort Clouds could enable investigators to link mass-loss from a white dwarf progenitor with the cometary population of the resulting white dwarf (see Alcock et al. 1986; Parriott & Alcock 1998). Additionally, one should also consider the difference in the stellar wind velocity at Oort Cloud distances versus its escape velocity when it leaves the star. As observed by Debes & Sigurdsson (2002), because the wind crossing time is typically longer than the Oort Cloud orbital time-scale, winds that have slowed will enhance the system's adiabaticity.

4.2 Wide-orbit planets

Initially, exoplanet discovery techniques were not well suited for detecting planets that reside beyond ≈6 au on decade-long time-scales, and this region remained relatively unexplored until the mid-2000s. However, new observational techniques and carefully targeted surveys are increasing the likelihood of uncovering planets on wide orbits (e.g. Crepp & Johnson 2011). The discoveries of the four planets with $a \approx 15, 24, 38, 68$ au orbiting HR 8799 (Marois et al. 2008, 2010) and the $a \approx 115$ au planet orbiting Formalhaut (Kalas et al. 2008) revealed that wide-orbit ($a >$ 10–100 au) planets do exist and incited great interest in their formation and evolution. Additionally, at least 10 wider orbit companions, which may be massive planets that are close to the brown dwarf mass limit, have been detected. Like Formalhaut b, the companion to GQ Lup (Guenther et al. 2005) is thought to satisfy $100 < a < 200$ au. Companions around AB Pic (Chauvin et al. 2005), Oph 11 (Close et al. 2007) and CHXR 73 (Luhman et al. 2006) – all harbour semimajor axis between 200 and 300 au, and those orbiting CT Cha (Schmidt et al. 2008), 1RXS J160929.1−210524 (Lafrenière, Jayawardhana & van Kerkwijk 2010) and GSC 06214−00210 (Ireland et al. 2011) satisfy $300 < a < 500$ au. Companions with $500 < a <$ 1000 au include those orbiting UScoCTIO 108 (Béjar et al. 2008), HIP 78530 (Lafrenière et al. 2011) and HN Peg B (Leggett et al. 2008). The three potentially planetary companions with the widest known orbits are SR 12 C (1100 au, Kuzuhara et al. 2011), Ross 458 b (1168 au, Goldman et al. 2010) and WD 0806−661B b (2500 au, Luhman, Burgasser & Bochanski 2011). Theoretical models place the mass of the $a = 2500$ au object at 7 Jupiter masses. Our study is particularly relevant to such wide-orbit companions.

During stellar evolution, wide-orbit planets in isolation will behave equivalently to Oort Cloud comets, and can be ejected with similar ease. Planets may be mutually scattered out to distances of $\sim 10^5$ au while remaining bound to their parent systems (Veras, Crepp & Ford 2009); beyond this distance, over time the effects of passing stars are likely to strip the planet from the system. Another mechanism for producing wide-orbit planets is capture from other stars, or passing free-floaters. There is still a possibility that the Sun contains a massive, very wide orbit companion. Fernández (2011) discusses the prospects for detecting a wide-orbit (>10^4 au) Jovian

mass companion to the Sun, and Matese & Whitmire (2011) suggest that there is evidence for such a companion residing in the Sun's outer Oort Cloud. Regardless, such planets are very unlikely to have formed in these environments; neither core accretion nor gravitational instability formation models can fully form planets beyond $\sim$100 au (Dodson-Robinson et al. 2009). Embryos and/or partially formed planets that were scattered beyond $\sim 10^3$–10^5 au will undergo the same dynamical evolution due to stellar mass-loss as a fully formed planet. This situation might arise around short-lived, high-mass stars, where the time-scale for core accretion might be longer than the mass-loss time-scale.

4.3 Multiple planets

Introducing additional bodies to the system, such as a second planet, or a belt of material, could significantly complicate the evolution. Debes & Sigurdsson (2002) investigate the first scenario, and Bonsor, Mustill & Wyatt (2011) the second. In both cases, the characteristics of their N-body simulations demonstrated that the systems they studied were in the adiabatic regime. In this regime, where stellar mass-loss produces quiescent adiabatic eccentricity excitation of the order of Ψ_0 (see equation 17), the eccentricity variation of the second planet or belt particles can then be attributed solely to the other planet. Additionally, the orbit of the true anomaly is only negligibly affected by mass-loss in the adiabatic limit. Thus, the main contribution of the stellar mass-loss in their studies is through the well-defined (equation 2) increase in semimajor axis of all objects in the system.

Including additional planets in situations where $\Psi_{\rm bif}$ is reached and/or exceeded represents several of the numerous potential extensions to this work. The frequency of planet–planet scattering and the resulting free-floating planet population in the midst of semimajor axis and eccentricity variations from stellar mass-loss are important issues to be addressed. Other situations to consider are how planets may stay locked into or be broken from secular and mean motion resonances, and how instability time-scales are affected.

4.4 Free-floating planets

The ejection of planetary material, whether it is in the form of partially formed planets, fully formed planets, or comets, might contribute to the free-floating mass present and potentially detectable around dead stars. Evidence for the existence of free-floating planets has been mounting (Lucas & Roche 2000; Zapatero Osorio et al. 2000, 2002; Bihain et al. 2009) and was recently highlighted by a report of potential detections of 10 free-floating planets (Sumi et al. 2011). Also, the capability may exist to distinguish between free-floaters and bound wide-orbit planets up to semimajor axes of $\approx$100 au (Han 2006).

Assuming that the same amount of planetary material was distributed equally among stars of all progenitor masses, then $\approx$7–20 $M_\odot$ progenitors are by far the most likely stars to produce free-floating material,[6] followed by stars in the $\approx$4–8 $M_\odot$ progenitor mass range (see Fig. 14). The ability of stars with $\mu_0 \gtrsim 20\,M_\odot$ to produce free floating material is unclear and is largely dependent on the evolutionary models used. For a given progenitor mass, metal-poor and/or metal-rich stars may be prone to ejecting planets. However, because metal-rich stars are slightly more likely to harbour planets than metal-poor stars (Setiawan et al. 2010), the metal-poor stars which are dynamically prone to planetary excitation might not initially harbour planets.

Detailed modelling of the Galaxy's free-floating planet population requires (1) an initial mass function; (2) better statistics for planets orbiting stars other than Sun-like hosts; (3) knowledge of how many planets inhabit wide orbits at for example, $a = 10^{3-5}$ au; and (4) a better knowledge of the ability for $\approx$1–2 $M_\odot$ stellar-mass progenitors to eject planets. Depending on these results, stellar evolution might be the primary source of free-floating planets. Alternatively, if, for example, a negligible number of planets are shown to inhabit orbits beyond $a = 10^3$ au, then the dominant source of free-floating planets would likely lie elsewhere.

4.5 Pulsar planets

Our results suggest that very few first-generation pulsar planets exist. Such planets would have had to reside far enough away from the expanding progenitor envelope to not be disrupted pre-supernova, and then survive the supernova. Assuming a uniform distribution of true anomalies, only $(180^\circ - f_{\rm crit})/180^\circ \approx 11$ per cent of planets would have a fighting chance to survive due to the additional time they would take to initially decrease their eccentricities. Even then, their initial eccentricities would have to be high enough, and the mass-loss duration short enough, to outlast the supernova. These results suggest that unless pulsars can readily form planets or capture them from other systems, pulsar planets should be relatively rare.

However, if the pulsar planet survived engulfment from the expanding pre-supernova stellar envelope, then its semimajor axis might be small enough to remain bound during the supernova. There is one planet, HIP 13044 (Setiawan et al. 2010), which potentially could have survived residing inside its star's envelope (Bear, Soker & Harpaz 2011). The spiral-in time of the planet could have exceeded the short duration ($\sim$100 yr) of the RGB expansion and engulfment, allowing the planet to survive. If close-in ($\lesssim$1 au) pulsar planets survive in a similar way, their final eccentricities could be any value (see Fig. 11) but their semimajor axes will have increased by many factors. The three pulsar planets orbiting PSR1257+12 (Wolszczan & Frail 1992; Wolszczan 1994) all have $a < 0.5$ au. If they are first-generation planets, then $a_0 \lesssim 0.1$ would have held true for each. At such a small semimajor axis, their resulting dynamical evolution during supernova would be approximately in the adiabatic-runaway transition region ($\Psi \sim 0.1$–1). The result is that their pre-Supernova eccentricities (which were probably nearly zero due to tidal circularization) could have been excited by a few hundredths to a few tenths, but not by enough to have suffered ejection. Although such values fit the observations, the system is significantly complicated by the mutual interactions amongst all the three planets, including a resonance locking. Instead, the observed pulsar planets may be second-generation planets (Perets 2010), i.e., captured (or even formed) after the supernova occurred.

4.6 Stellar properties

Other questions to consider focus on the star itself. How does non-constant multiphase mass-loss affect the results here? Non-isotropic and/or asymmetric mass-loss may have a drastic influence on the resulting cometary (Parriott & Alcock 1998) and planetary (Namouni 2005; Namouni & Zhou 2006) evolution. In this case, the system no

[6] One potential indication of the origin of supernova-produced free-floaters is their space velocities; neutron star 'kicks' cause the true space velocities of young pulsars to reflect the (high) speed of the supernova ejecta (Hobbs et al. 2005).

longer conserves angular momentum, and new equations of motion must be derived. How do short bursts, periodic or not, of ejected mass accompanying pulsating stars affect the planetary orbit? In this case, planetary evolution may even undergo several transitions between the adiabatic and runaway regimes. The expansion and/or contraction of the stellar envelope and the resulting tidal effects on surviving planets could also play an important role in some cases. Tides will compete with planetary ejection and possibly eccentricity excitation. Further, planets could be expanding their semimajor axes – and their Hill Spheres – as they are experiencing tidal effects *and* competing with the expanding stellar envelope. Some exoplanets will likely be evaporated while others will travel through the stellar envelope, accreting mass and being subject to a possible non-isotropic mass distribution of the stellar envelope.

5 CONCLUSION

The variable-mass two-body problem allows for the bodies to become unbound or highly eccentric. The implications of this physical principle affect all dying stellar systems which contain any orbiting material. Many Oort Clouds and many wide-orbit planets will have their orbits disrupted. The extent of the disruption depends crucially on their initial semimajor axes, eccentricities and true anomalies, and the subtleties of stellar evolution. Stars with progenitor masses of 4–8 $M_{\odot}$ will readily eject objects that are beyond a few hundred au distant, and excite the eccentricities of the remaining bound material at that distance. Supernovae that produce neutron stars eject nearly but not all orbiting material. Conversely, other exotic systems, such as those with black holes, could have easily retained planets during their formation. Stellar mass-loss might be the dominant source of the free-floating planet population, and orbital properties of currently observed disrupted planets in aged systems may be tracers of the evolution of their parent stars.

ACKNOWLEDGMENTS

We thank the referee for helpful suggestions, and Mukremin Kilic, Christopher A. Tout and Kimberly A. Phifer for useful discussions and references.

REFERENCES

Alcock C., Fristrom C. C., Siegelman R., 1986, ApJ, 302, 462
Bear E., Soker N., 2011, MNRAS, 411, 1792
Bear E., Soker N., Harpaz A., 2011, ApJ, 733, L44
Béjar V. J. S., Zapatero Osorio M. R., Pérez-Garrido A., Álvarez C., Martín E. L., Rebolo R., Villó-Pérez I., Díaz-Sánchez A., 2008, ApJ, 673, L185
Belczynski K., Bulik T., Fryer C. L., Ruiter A., Valsecchi F., Vink J. S., Hurley J. R., 2010, ApJ, 714, 1217
Benatti S. et al., 2010, preprint (arXiv:1012.0747)
Beuermann K. et al., 2011, A&A, 526, A53
Bihain G. et al., 2009, A&A, 506, 1169
Bonsor A., Mustill A., Wyatt M., 2011, MNRAS, 414, 930
Brasser R., Higuchi A., Kaib N., 2010, A&A, 516, A72
Butler R. P., Tinney C. G., Marcy G. W., Jones H. R. A., Penny A. J., Apps K., 2001, ApJ, 555, 410
Chambers J. E., 1999, MNRAS, 304, 793
Chauvin G. et al., 2005, A&A, 438, L29
Chauvin G., Lagrange A.-M., Udry S., Fusco T., Galland F., Naef D., Beuzit J.-L., Mayor M., 2006, A&A, 456, 1165
Clark J. S., Goodwin S. P., Crowther P. A., Kaper L., Fairbairn M., Langer N., Brocksopp C., 2002, A&A, 392, 909
Close L. M. et al., 2007, ApJ, 660, 1492
Crepp J. R., Johnson J. A., 2011, ApJ, 733, 126
Crowther P. A., Schnurr O., Hirschi R., Yusof N., Parker R. J., Goodwin S. P., Kassim H. A., 2010, MNRAS, 408, 731
Debes J. H., Sigurdsson S., 2002, ApJ, 572, 556
Deprit A., 1983, Celest. Mech., 31, 1
Desidera S., Barbieri M., 2007, A&A, 462, 345
Dessart L., Livne E., Waldman R., 2010, MNRAS, 408, 827
Di Stefano R., Howell S. B., Kawaler S. D., 2010, ApJ, 712, 142
Dodson-Robinson S. E., Veras D., Ford E. B., Beichman C. A., 2009, ApJ, 707, 79
Drake A. J. et al., 2010, preprint (arXiv:1009.3048)
Duncan M., Quinn T., Tremaine S., 1987, AJ, 94, 1330
Dybczyński P. A., 2002, A&A, 396, 283
Efroimsky M., 2005a, Celest. Mech. Dynamical Astron., 91, 75
Efroimsky M., 2005b, Ann. New York Acad. Sci., 1065, 346
Efroimsky M., 2006, Celest. Mech. Dynamical Astron., 96, 259
Efroimsky M., Goldreich P., 2003, J. Math. Phys., 44, 5958
Efroimsky M., Goldreich P., 2004, A&A, 415, 1187
Eldridge J. J., Tout C. A., 2004, MNRAS, 353, 87
Faedi F., West R. G., Burleigh M. R., Goad M. R., Hebb L., 2011, MNRAS, 410, 899
Fernández J. A., 2011, ApJ, 726, 33
Fesen R. A., Höflich P. A., Hamilton A. J. S., Hammell M. C., Gerardy C. L., Khokhlov A. M., Wheeler J. C., 2007, ApJ, 658, 396
Fryer C. L., 1999, ApJ, 522, 413
Gardner E., Nurmi P., Flynn C., Mikkola S., 2011, MNRAS, 411, 947
Geier S., Edelmann H., Heber U., Morales-Rueda L., 2009, ApJ, 702, L96
Goldman B., Marsat S., Henning T., Clemens C., Greiner J., 2010, MNRAS, 405, 1140
Guenther E. W., Neuhäuser R., Wuchterl G., Mugrauer M., Bedalov A., Hauschildt P. H., 2005, Astron. Nachr., 326, 958
Gurfil P., 2004, Celest. Mech. Dynamical Astron., 90, 289
Gurfil P., 2007, Acta Astronautica, 60, 61
Gurfil P., Belyanin S., 2008, Advances Space Res., 42, 1313
Gyldén H., 1884, Astron. Nachr., 109, 1
Hadjidemetriou J. D., 1963, Icarus, 2, 440
Hadjidemetriou J. D., 1966a, Icarus, 5, 34
Hadjidemetriou J. D., 1966b, Z. Astrophys., 63, 116
Hamann W.-R., Koesterke L., Wessolowski U., 1995, A&A, 299, 151
Hamuy M., Pinto P. A., 2002, ApJ, 566, L63
Han C., 2006, ApJ, 644, 1232
Hansen B. M. S., 2010, ApJ, 723, 285
Heger A., Fryer C. L., Woosley S. E., Langer N., Hartmann D. H., 2003, ApJ, 591, 288
Higuchi A., Kokubo E., Kinoshita H., Mukai T., 2007, AJ, 134, 1693
Hills J. G., 1981, AJ, 86, 1730
Hobbs G., Lorimer D. R., Lyne A. G., Kramer M., 2005, MNRAS, 360, 974
Hogan E., Burleigh M. R., Clarke F. J., 2009, MNRAS, 396, 2074
Humphreys R. M., Davidson K., 1994, PASP, 106, 1025
Hurley J. R., Pols O. R., Tout C. A., 2000, MNRAS, 315, 543
Iorio L., 2010, Nat. Sci., 2, 329
Ireland M. J., Kraus A., Martinache F., Law N., Hillenbrand L. A., 2011, ApJ, 726, 113
Jeans J. H., 1924, MNRAS, 85, 2
Kaib N. A., Quinn T., 2008, Icarus, 197, 221
Kalas P. et al., 2008, Sci, 322, 1345
Kalogera V., Baym G., 1996, ApJ, 470, L61
Kudritzki R. P., Reimers D., 1978, A&A, 70, 227
Kuzuhara M., Tamura M., Ishii M., Kudo T., Nishiyama S., Kandori R., 2011, AJ, 141, 119
Lafrenière D., Jayawardhana R., van Kerkwijk M. H., 2010, ApJ, 719, 497
Lafrenière D., Jayawardhana R., Janson M., Helling C., Witte S., Hauschildt P., 2011, ApJ, 730, 42
Lagrange A.-M., Beust H., Udry S., Chauvin G., Mayor M., 2006, A&A, 459, 955
Lee J. W., Kim S.-L., Kim C.-H., Koch R. H., Lee C.-U., Kim H. I., Park J.-H., 2009, AJ, 137, 3181
Leggett S. K. et al., 2008, ApJ, 682, 1256

Leto G., Jakubík M., Paulech T., Neslušan L., Dybczyński P. A., 2008, MNRAS, 391, 1350
Levison H. F., Duncan M. J., Brasser R., Kaufmann D. E., 2010, Sci, 329, 187
Li L.-S., 2008, Astron. Rep., 52, 806
Lucas P. W., Roche P. F., 2000, MNRAS, 314, 858
Luhman K. L. et al., 2006, ApJ, 649, 894
Luhman K. L., Burgasser A. J., Bochanski J. J., 2011, ApJ, 730, L9
Marois C., Macintosh B., Barman T., Zuckerman B., Song I., Patience J., Lafrenière D., Doyon R., 2008, Sci, 322, 1348
Marois C., Zuckerman B., Konopacky Q. M., Macintosh B., Barman T., 2010, Nat, 468, 1080
Massarotti A., 2008, AJ, 135, 2287
Matese J. J., Whitmire D. P., 2011, Icarus, 211, 926
Mayor M., Udry S., Naef D., Pepe F., Queloz D., Santos N. C., Burnet M., 2004, A&A, 415, 391
Mazzali P. A., Maurer I., Valenti S., Kotak R., Hunter D., 2010, MNRAS, 408, 87
Mestschersky J., 1893, Astron. Nachr., 132, 129
Mugrauer M., Neuhäuser R., 2005, MNRAS, 361, L15
Mullally F., Winget D. E., De Gennaro S., Jeffery E., Thompson S. E., Chandler D., Kepler S. O., 2008, ApJ, 676, 573
Mullally F., Reach W. T., De Gennaro S., Burrows A., 2009, ApJ, 694, 327
Namouni F., 2005, AJ, 130, 280
Namouni F., Zhou J. L., 2006, Celest. Mech. Dynamical Astron., 95, 245
Nieuwenhuijzen H., de Jager C., 1990, A&A, 231, 134
Nordhaus J., Spiegel D. S., Ibgui L., Goodman J., Burrows A., 2010, MNRAS, 408, 631
O'Connor E., Ott C. D., 2011, ApJ, 730, 70
Parriott J., Alcock C., 1998, ApJ, 501, 357
Perets H. B., 2010, preprint (arXiv:1001.0581)
Plastino A. R., Muzzio J. C., 1992, Celest. Mech. Dynamical Astron., 53, 227
Qian S.-B., Liao W.-P., Zhu L.-Y., Dai Z.-B., Liu L., He J.-J., Zhao E.-G., Li L.-J., 2010a, MNRAS, 401, L34
Qian S.-B., Liao W.-P., Zhu L.-Y., Dai Z.-B., 2010b, ApJ, 708, L66
Qian S.-B. et al., 2011, MNRAS, 414, L16
Queloz D. et al., 2000, A&A, 354, 99
Rahoma W. A., Abd El-Salam F. A., Ahmed M. K., 2009, JA&A, 30, 187
Razbitnaya E. P., 1985, SvA, 29, 6
Rybicki K. R., Denis C., 2001, Icarus, 151, 130
Sackmann I.-J., Boothroyd A. I., Kraemer K. E., 1993, ApJ, 418, 457
Schmidt T. O. B., Neuhäuser R., Seifahrt A., Vogt N., Bedalov A., Helling C., Witte S., Hauschildt P. H., 2008, A&A, 491, 311
Schröder K.-P., Connon Smith R., 2008, MNRAS, 386, 155
Schröder K.-P., Cuntz M., 2005, ApJ, 630, L73
Schuh S. et al., 2010, Ap&SS, 329, 231
Setiawan J., Klement R. J., Henning T., Rix H.-W., Rochau B., Rodmann J., Schulze-Hartung T., 2010, Sci, 330, 1642
Sigurdsson S., Richer H. B., Hansen B. M., Stairs I. H., Thorsett S. E., 2003, Sci, 301, 193
Silvotti R. et al., 2007, Nat, 449, 189
Smartt S. J., Eldridge J. J., Crockett R. M., Maund J. R., 2009, MNRAS, 395, 1409
Strobel K., Weigel M. K., 2001, A&A, 367, 582
Sumi T. et al., 2011, Nat, 473, 349
Szalai T., Vinkó J., Balog Z., Gáspár A., Block M., Kiss L. L., 2011, A&A, 527, A61
Vassiliadis E., Wood P. R., 1993, ApJ, 413, 641
Veras D., Crepp J. R., Ford E. B., 2009, ApJ, 696, 1600
Verhulst F., 1969, Bull. Astron. Inst. The Netherlands, 20, 215
Verhulst F., 1972, Celest. Mech., 5, 27
Verhulst F., Eckhaus W., 1970, Int. J. Non-linear Mech., 5, 617
Villaver E., Livio M., 2007, ApJ, 661, 1192
Villaver E., Livio M., 2009, ApJ, 705, L81
Wickramasinghe D. T., Farihi J., Tout C. A., Ferrario L., Stancliffe R. J., 2010, MNRAS, 404, 1984
Wolszczan A., 1994, Sci, 264, 538
Wolszczan A., Frail D. A., 1992, Nature, 355, 145
Woosley S. E., Langer N., Weaver T. A., 1993, ApJ, 411, 823
Woosley S. E., Heger A., Weaver T. A., 2002, Rev. Modern Phys., 74, 1015
Yoon S.-C., Cantiello M., 2010, ApJ, 717, L62
Zapatero Osorio M. R., Béjar V. J. S., Martín E. L., Rebolo R., Barrado y Navascués D., Bailer-Jones C. A. L., Mundt R., 2000, Sci, 290, 103
Zapatero Osorio M. R., Béjar V. J. S., Martín E. L., Rebolo R., Barrado y Navascués D., Mundt R., Eislöffel J., Caballero J. A., 2002, ApJ, 578, 536
Zhang W., Woosley S. E., Heger A., 2008, ApJ, 679, 639

This paper has been typeset from a TEX/LATEX file prepared by the author.